University Library

A gateway to Melbourne's research publications

Minerva Access is the Institutional Repository of The University of Melbourne

Author/s:
Bishop, CH;Frolov, S;Allen, DR;Kuhl, DD;Hoppel, K

Title:
The Local Ensemble Tangent Linear Model: an enabler for coupled model 4D-Var

Date:
2017

Citation:
Bishop, C. H., Frolov, S., Allen, D. R., Kuhl, D. D. & Hoppel, K. (2017). The Local Ensemble Tangent Linear Model: an enabler for coupled model 4D-Var. Quarterly Journal of the Royal Meteorological Society, 143 (703), pp.1009-1009. https://doi.org/10.1002/qj.2986.

Persistent Link:
https://hdl.handle.net/11343/292295

The Local Ensemble Tangent Linear Model: an enabler for coupled model 4DVAR

Craig H. Bishop

Marine Meteorology Division, Naval Research Laboratory, Monterey, CA

Sergey Frolov

University Corporation for Atmospheric Research, Monterey, CA

Douglas R. Allen, David D. Kuhl, Karl Hoppel

Remote Sensing Division, Naval Research Laboratory, Washington DC

Author Manuscript

This is the author manuscript accepted for publication and has undergone full peer review but has not been through the copyediting, typesetting, pagination and proofreading process, which may lead to differences between this version and the Version of Record. Please cite this article as doi: 10.1002/qj.2986

This article is protected by copyright. All rights reserved.

Author Manuscript

Abstract

A leading Data Assimilation (DA) technique in meteorology is 4DVAR which relies on the Tangent Linear Model (TLM) of the non-linear model and its adjoint. The difficulty of building and maintaining traditional TLMs and adjoints of coupled ocean-wave-atmosphere-etc models is daunting. On the other hand, coupled model ensemble forecasts are readily available. Here, we show how an ensemble forecast can be used to construct an accurate Local Ensemble TLM (LETLM) and adjoint of the entire coupled system. The method features a local influence region containing all the variables that could possibly influence the time evolution of some target variable(s) near the center of the region. We prove that high accuracy is guaranteed provided that (i) the ensemble perturbations are governed by linear dynamics, and (ii) the number of ensemble members exceeds the number of variables in the influence region. The approach is illustrated in a simple coupled model. This idealized coupled model has some realistic features including reasonable predictability limits in the upper-atmosphere, lower-atmosphere, upper-ocean and lower-ocean of 10, 96, 160 and 335 days, respectively. In addition, the length scale of eddies in the ocean is about one fifth of those in the atmosphere. The easy manner in which the adjoint is obtained from the LETLM is also described and illustrated by demonstrating how the LETLM adjoint predicts the high sensitivity of oceanic boundary layer evolution to changes in the atmosphere. Finally, the feasibility of LETLMs for 4DVAR is demonstrated. Specifically, a case

This article is protected by copyright. All rights reserved.

is considered with a 5 day data assimilation window in which non-linear terms play a significant role in the evolution of forecast error; it is shown that the posterior mode delivered by 4DVAR with an LETLM, its adjoint and 10 outer loops approximately recovers the true state in spite of a spatially sparse observational network.

Author Manuscript

1. Introduction

Models of the atmosphere, land-surface, ice, wave, ocean and aerosols are coupled together for the purpose of climate modelling (McGuffie and Henderson-Sellers, 2005). Such model coupling is also essential for sub-seasonal (15-90 days), seasonal, annual and decadal environmental prediction (Saha et al. 2010; MacLachlan et al. 2014; Shelly et al. 2014). Aspects of short to medium range atmospheric forecasts such as the diurnal cycle, near surface temperatures around ice edges and precipitation can also all be significantly affected by such coupling (Chen et al. 2010; Smith et al. 2013). For these reasons, coupled ocean-atmosphere-wave-ice-land-aerosol models promise to increase the accuracy of environmental forecasts over a broad time horizon (Buizza and Leutbecher, 2015).

Relatively sophisticated uncoupled DA schemes have been developed for uncoupled sub-models of the coupled system such as the ocean and atmosphere. One can use these uncoupled models and DA schemes to initialize coupled model forecasts but a drawback of this approach is that observational information is propagated forward in time by the uncoupled models rather than the potentially superior coupled model. Mulholland et al. (2015) found that this approach

This article is protected by copyright. All rights reserved.

led to initialization shocks that degraded the quality of subsequent forecasts. A more satisfactory variation on this approach is to simply replace the uncoupled models' "first guess" of observations used in the uncoupled DA schemes by a first guess from the coupled model. This approach is called *weakly coupled DA*. In general, weakly coupled DA does not allow oceanic (atmospheric) observations to affect the analysis of the atmosphere (ocean). However, as shown by Laloyaux et al. (2015), if a 4DVAR outer-loop (Rabier et al., 2000, Rosmond and Xu, 2007, Gauthier et al., 2007) is employed, oceanic (atmospheric) observations do affect the atmospheric (oceanic) analysis. Thus, the outer loop turns a weakly coupled DA scheme into a *moderately coupled* DA scheme.

Since physics couples properties of each of the sub-components together, errors in the forecast of one component of the coupled model will covary with errors in other components. A DA scheme that uses a model of the error covariances between one or more sub-components of the coupled system is called a *strongly coupled* DA scheme and, in theory, the strongly coupled schemes should be more accurate than any of the other schemes. As discussed in Smith et al. (2015), if the TLM and adjoint of the full coupled model are employed in 4DVAR then such inter-fluid covariances will form within the 4DVAR window as a consequence of coupled model dynamics even if the initial inter-fluid covariances had been set to zero. Using Anderson's (2001, 2003) Ensemble Adjustment Filter, Zhang et al. (2007) describe a strongly coupled DA scheme in which a climate model was used to generate synthetic observations, which were subsequently assimilated using the Ensemble Adjustment Filter. A 4DVAR strongly coupled DA would feature an outer-loop just like that of Laloyaux et al. (2015) but unlike Laloyaux et al., it would

Author Manuscript

This article is protected by copyright. All rights reserved.

also feature a TLM and adjoint of the coupled model, and possibly, non-zero initial error covariances between model sub-components such as the atmosphere and ocean.

Currently, 4DVAR (Courtier et al., 1994) is used to produce initial conditions at many of the major medium range atmospheric forecasting centers (Rabier et al., 2000, Kadowaki, 2005, Xu et al., 2005, Rosmond and Xu., 2006, Rawlins et al., 2007, Gauthier et al., 2007). 4DVAR attempts to find the state that minimizes a penalty/cost function of the non-linear trajectory of the model using an estimate of the gradient of this cost-function with respect to the state. A key component of this gradient is the TLM and adjoint of a linearized version of the non-linear model. The construction and maintenance of a traditional TLM is non-trivial. The numerical stability of the non-linear model does not guarantee the numerical stability of the linear model. Sometimes a module of the non-linear model needs to be approximated in some way before its linearized counterpart will be numerically stable. Representations of sub-grid-scale processes often involve state dependent switches that abruptly change the tendency of the non-linear model. Such aspects of the model are formally non-differentiable and considerable testing may be required before a satisfactory approximation to the TLM of such processes can be obtained. Similarly extensive testing may also be required to obtain satisfactory TLM approximations to *stochastic* aspects of the model that are driven by random numbers. These challenges mean that it takes a significant amount of time to develop a satisfactory TLM. Once a TLM code has been developed to represent a reasonable TLM operator, one then needs to develop the corresponding adjoint code.

Author Manuscript

This article is protected by copyright. All rights reserved.

The time frame for TLM/adjoint development needs to be compared to the time frame of significant changes to the non-linear model. Ideally, one would build and maintain the TLM and adjoint of every sub-model and every sub-model coupler on a time frame shorter than the time frame with which changes are being made to the full coupled system. Not impossible but not easy.

One could choose to move to forms of 4DVAR that do not require a TLM/adjoint such as those described in Liu et al. (2008), Bishop and Hodyss (2011) and Buehner et al. (2013). These schemes replace the linearly propagated four dimensional forecast error covariance matrices of 4DVAR with localized four-dimensional ensemble covariances. However, Lorenc et al. (2015), showed that these no TLM/adjoint approaches do not perform as well as schemes that use TLM/adjoints when Hybrid initial error covariance models are used in the 4DVAR. Such Hybrid initial error covariance models blend localized ensemble covariances with static quasi-isotropic covariances and have been shown by Clayton et al. (2013) and Kuhl et al. (2013), amongst others, to significantly improve the performance of 4DVAR schemes that use TLM/adjoints.

An alternative approach to the development and maintenance of TLMs and their adjoints has recently been proposed by Frolov and Bishop (2016). Frolov and Bishop (2016) investigated a variety of different methods of approximating TLMs using ensemble forecasts. Their main focus was the effect of ensemble covariance localization on ensemble based TLM performance. Here, for the first time, we demonstrate that if the non-linear model is differentiable then there is a

Author Manuscript

This article is protected by copyright. All rights reserved.

Local Ensemble TLM (LETLM) that is identical to the true TLM provided that (i) the ensemble perturbations are small enough to be governed by the true TLM, and (ii) the number of ensemble members exceeds the number of variables that influence the tendency of a single model variable over a single time-step. The LETLM in this paper corresponds to the Ensemble-based TLM described in subsection (3.e) of Frolov and Bishop (2016). The name LETLM was chosen, in part, to emphasize the similarity between its numerical structure and Hunt et al.'s (2007) Local Ensemble Transform Kalman Filter (LETKF).

With accurate LETLM/adjoints, changes to the non-linear model that do not involve changing the model time step or model grids would not generally affect the accuracy of the LETLM/adjoint code. Non-linear model changes that did involve model time steps or model grids would only require relatively trivial changes to the LETLM influence volumes and/or ensemble sizes. This simplicity of TLM code development is one of the primary appeals of the LETLM approach to TLMs and their adjoints.

To emphasize the LETLMs suitability for coupled systems, a new 4-level coupled model was constructed by coupling versions of Lorenz's (2005) model 1 so that the resulting system would have qualitatively similar characteristics to a coupled ocean-atmosphere model. This model is described in detail in Section 2. Section 3 describes the LETLM and gives the analytical proof of the potential equivalence of the LETLM with the true TLM. Section 4 demonstrates the high degree of accuracy of the LETLM. Section 5 describes the simple procedure by which the adjoint of LETLM is constructed and uses it to compute the sensitivity of our idealized coupled model to

Author Manuscript

This article is protected by copyright. All rights reserved.

changes in initial conditions. Section 6 demonstrates the use of the LETLM and its adjoint in coupled model 4DVAR. Conclusions follow in Section 7.

2. Idealized coupled model

To provide a simple framework to test and evaluate strategies for coupled DA, a new idealized coupled model was created by coupling four realizations of model 1 of Lorenz (2005). The model has two atmospheric levels of 20 variables each and two oceanic levels of 100 variables each (see Figure 1). A detailed description of the equations governing the evolution of this model is given in the Appendix. The choices of the parameters used in the model were aimed at achieving quasi-realistic features such as (i) an upper-atmosphere with weak coupling to the ocean, relatively large scale chaotic waves and predictability time scales very similar to the atmosphere (~10 days) (ii) a lower atmospheric layer that is like a boundary layer in that it has moderate dynamic coupling to the upper ocean layer, chaotic waves of a similar scale to the upper atmosphere, but a significantly longer predictability time scale due to its coupling to a more slowly evolving ocean (iii) an upper most ocean level that is like an ocean mixed layer in that it has moderately dynamic coupling with the atmosphere but also supports chaotic waves of considerably smaller wavelength than those of the atmosphere, and (iv) a deep ocean layer that has relatively weak coupling to all other layers, long predictability time-scales and slowly evolving chaotic waves of a much smaller length scale than those of the atmosphere. The horizontal lateral boundary conditions for all four levels of the model are periodic.

Author Manuscript

This article is protected by copyright. All rights reserved.

To spin-up the model it was initialized with random noise and integrated for 1,000 six hr time steps. (The time step is the same for both the ocean and the atmosphere). Visual inspection of the evolution of the state over this time indicated that the spatio-temporal scales of the chaotic model were stabilized after this period.

After this spin-up period, the model was integrated for another 10,000 six hr time steps and the model state was saved at every time step. Experimentation to be discussed later showed that all predictability is lost in this model in less than 365 days. This suggests that the 2500 day integration corresponding to the 10,000 time steps is sufficient to reasonably sample the climatology of this model. A uniform sample of 500 was obtained from this climatology of states by selecting every 20^{th} entry from the 10,000 states. The first 480 of these 500 selected states are described by the black lines on Figure 1. (This 480 member subset was thought sufficient to define a large and state-space spanning ensemble as this number is equal to twice the number of model variables). These states can be viewed as a 480 member sample of the climatology of our idealized model. The red line on Figure 1 depicts a randomly selected state taken from this sample. The red line on figure 1 indicates that, as desired, (i) the horizontal scale of the atmospheric variations at both atmospheric levels is significantly longer than that of the corresponding variations in the deepest ocean, and (ii) the scales of perturbations found in the upper ocean layer share characteristics of the short scale deep ocean disturbances and the larger scale atmospheric disturbances. For future reference, we note that we also created a distinct set of 500 climatological states by again selecting every 20^{th} state from our sample of 10,000 but this

Author Manuscript

This article is protected by copyright. All rights reserved.

time we let the first state in the list of 500 be the 10^{th} state from the list of 10,000 rather than the first member. The states in this second set are all separated from the first set by at least 9 time steps. We used the first set for generating initial ensemble members and the second set for generating a random realization of truth.

To indicate the predictability characteristics of the coupled model, an ensemble was created after the spin-up period by adding random perturbations to the truth. The random perturbations were chosen to have exactly the same covariance structure as the climatological covariance of the model evolution over a very long time period. However, their amplitude was chosen to be much smaller than climatological perturbations. Specifically, the i^{th} initial ensemble member $\mathbf{x}_i$ was generated from a coupled model state $\mathbf{x}^t$ by the random process

$$\mathbf{x}_i = \mathbf{x}^t + \frac{1}{100}\left(\mathbf{P}^c\right)^{1/2} \eta_i \qquad (1)$$

where $\left(\mathbf{P}^c\right)^{1/2}$ is the square root of the climatological covariance matrix and η_i is a random normal vector drawn from a distribution with a mean of zero and a covariance matrix equal to the identity matrix; in other words, $\eta_i \sim N(\mathbf{0},\mathbf{I})$. The 480 columns of the matrix $\left(\mathbf{P}^c\right)^{1/2}$ were simply given by the deviations of 480 random climatological states about their sample mean divided by the square root of 479. Note that the initial covariance matrix of an ensemble generated using (1) is 10^{-4} of the climatological covariance and hence the perturbations can be considered to be small.

Author Manuscript

This article is protected by copyright. All rights reserved.

To study the predictability of our coupled model in a computationally efficient manner, just sixteen ensemble members were created using (1) and then to ensure that the ensemble and true state were drawn from exactly the same distribution, equation (1) was used to generate a new truth that was independent of the 16 ensemble members. Figure 2 shows the evolution of the horizontally averaged sample variance of this ensemble together with the evolution of the horizontally averaged square of the difference between the sample mean and the truth. It illustrates how both the ensemble variance and mean square error of the ensemble mean grow in time for an extended period before saturating at the climatological variance of the coupled model. The growth happens most rapidly in the upper atmospheric layer and most slowly in the deep ocean layer. Note that the mean square error and ensemble variance are approximately equal to each other throughout the integration.

If we define the practical loss of predictability to occur at the time at which the variance of this ensemble grows to 99% of its value at the end of the 360 days of integration then predictability is lost in the upper-atmosphere, lower-atmosphere, upper-ocean and lower-ocean after 10, 96, 160 and 335 days, respectively.

3. The LETLM and the true TLM

In finite difference and finite volume models, the change in a variable's value over a time step is determined by the values of variables in a very near neighborhood of the variable in question. The precise number of variables contributing to the time change depends on the order

Author Manuscript

This article is protected by copyright. All rights reserved.

of the finite difference approximations to spatial derivatives and to the type of time stepping scheme employed. Figure 3 heuristically summarizes the situation for a 2D model. Specifically, the black circle on Figure 3 defines an LETLM influence volume. This influence volume contains, at a minimum, all of the variables that will influence the future time state of the variable at the center of the influence volume.

More generally, suppose that there are n variables at time t in the influence volume that influence the later time $t+\delta t$ value of the central m^{th} model variable, which we will denote by $x_m\left(t+\delta t\right)$. Further suppose that, at the initial time t, one had a K-member ensemble forecast which had small mean square distance $\sigma^2_{\max}$ around the time t influence volume guess field $\left[x_1^g, x_2^g, \cdots, x_n^g\right]$. Then provided the influence region contains all the variables used by the non-linear model to update the m^{th} variable,

$$\begin{aligned}&\left[x_{m1}\left(t+\delta t\right), x_{m2}\left(t+\delta t\right), ..., x_{mK}\left(t+\delta t\right)\right]\\ &= \left[M_m\left(\begin{bmatrix} x_1^g+\delta x_{11} \\ x_2^g+\delta x_{21} \\ \vdots \\ x_n^g+\delta x_{n1}\end{bmatrix}\right), M_m\left(\begin{bmatrix} x_1^g+\delta x_{12} \\ x_2^g+\delta x_{22} \\ \vdots \\ x_n^g+\delta x_{n2}\end{bmatrix}\right), \cdots, M_m\left(\begin{bmatrix} x_1^g+\delta x_{1K} \\ x_2^g+\delta x_{2K} \\ \vdots \\ x_n^g+\delta x_{nK}\end{bmatrix}\right)\right]\end{aligned} \qquad (2)$$

where M_m is the part of the non-linear model that determines the future time state of the m^{th} variable from the n variables in the influence volume and where $\left[x_1^g, x_2^g, \cdots, x_n^g\right]$ and

Author Manuscript

This article is protected by copyright. All rights reserved.

$\left[x_1^g + \delta x_{1j}, x_2^g + \delta x_{2j}, \cdots, x_n^g + \delta x_{nj}\right]$ denote the values of the unperturbed guess and the j[th] perturbed guess of the true values at time t within the *n*-variable influence region.

TLM models are defined as perturbations to a guess trajectory. The guess trajectory corresponding to each ensemble perturbation is given by

$$\left[x_m^g\left(t+\delta t\right), x_m^g\left(t+\delta t\right), ..., x_m^g\left(t+\delta t\right)\right] = \left[M_m\left(\begin{bmatrix} x_1^g \\ x_2^g \\ \vdots \\ x_n^g \end{bmatrix}\right), M_m\left(\begin{bmatrix} x_1^g \\ x_2^g \\ \vdots \\ x_n^g \end{bmatrix}\right), \cdots, M_m\left(\begin{bmatrix} x_1^g \\ x_2^g \\ \vdots \\ x_n^g \end{bmatrix}\right)\right] \quad (3)$$

Without loss of generality, one can represent the local non-linear model in terms of a Taylor expansion of operators on the ensemble perturbations (for example, equation 3 of Julier and Uhlmann, 2004). In the limit of vanishingly small ensemble perturbations (i.e. when $\sigma_{\max}^2 \to 0$) only the linear operator within this expansion is non-negligible and subtracting equation (3) from (2) yields

$$\left[\delta x_{m1}\left(t+\delta t\right), \delta x_{m2}\left(t+\delta t\right), ..., \delta x_{mK}\left(t+\delta t\right)\right] = \mathbf{M}_m\left(i+1, i\right)\begin{bmatrix} \delta x_{11}, \delta x_{12}, ..., \delta x_{1K} \\ \delta x_{21}, \delta x_{22}, ..., \delta x_{2K} \\ \vdots \\ \delta x_{n1}, \delta x_{n2}, ..., \delta x_{nK} \end{bmatrix}, \quad (4)$$

Author Manuscript

This article is protected by copyright. All rights reserved.

where $\delta x_{mj}\left(t+\delta t\right)=x_{mj}\left(t+\delta t\right)-x_m^g\left(t+\delta t\right)$ and where $\mathbf{M}_m\left(i+1,i\right)$ is the true Local TLM for the m^{th} grid point for the evolution of a perturbation from the i^{th} time step to the $(i+1)^{\text{th}}$ time step. $\mathbf{M}_m\left(i+1,i\right)$ has one row and n columns. Defining

$$\Xi_m=\left[\delta x_{m1}\left(t+\delta t\right),\delta x_{m2}\left(t+\delta t\right),...,\delta x_{mK}\left(t+\delta t\right)\right] \text{ and } \mathbf{X}_m=\begin{bmatrix}\delta x_{11},\delta x_{12},...,\delta x_{1K}\\ \delta x_{21},\delta x_{22},...,\delta x_{2K}\\ \vdots\\ \delta x_{n1},\delta x_{n2},...,\delta x_{nK}\end{bmatrix}. \quad (5)$$

Note that in (5) and throughout this paper, we use italic fonts to identify scalars and bold fonts to identify vectors and matrices. Thus, a bold font subscripted by m indicates a matrix or vector whose variables cover the entire m^{th} influence region whereas a scalar subscripted by m indicates the m^{th} scalar target variable to be time stepped by the LETLM.

Eq. (4) can be rewritten in the form

$$\Xi_m=\mathbf{M}_m\left(i+1,i\right)\mathbf{X}_m \quad (6)$$

Note that if the nxn matrix $\left(\mathbf{X}_m\mathbf{X}_m^T\right)$ has an inverse then right multiplying (6) by $\mathbf{X}_m^T$ and then solving the resulting equation for $\mathbf{M}_m$ gives

$$\mathbf{M}_m\left(i+1,i\right)=\Xi_m\mathbf{X}_m^T\left(\mathbf{X}_m\mathbf{X}_m^T\right)^{-1} \quad (7)$$

Author Manuscript

This article is protected by copyright. All rights reserved.

Now the inverse $\left(\mathbf{X}_m\mathbf{X}_m^T\right)^{-1}$ is guaranteed to exist provided that the matrix $\mathbf{X}_m$ has n non-zero singular values. In a well formed ensemble, K-1 ensemble members will be linearly independent. Hence, with well-formed ensemble members (7) will precisely recover the true local TLM $\mathbf{M}_m\left(i+1,i\right)$ when $K \geq n+1$. In strong-constraint 4DVAR, the TLM is only used to propagate perturbations that lie in the vector sub-space spanned by the eigenvectors of the background error covariance matrix **B** that have non-zero eigenvalues. If the corresponding error sub-space in the influence region can be spanned with just q vectors where $q<n$, then well-formed ensembles with just $K \geq q+1$ would be sufficient to perfectly describe the true local TLM. Thus, a perfect ensemble TLM may be possible with fewer ensemble members K than influence region variables n when **B** has zero eigenvalues. If $K < n+1$ then the inverse in (7) would need to be replaced by a pseudo-inverse (Frolov and Bishop, 2016); furthermore, with $K < n+1$ an equivalent but more computationally efficient form of (7) is

$$\mathbf{M}_m\left(i+1,i\right) = \Xi_m\left(\mathbf{X}_m^T\mathbf{X}_m\right)^{-1}\mathbf{X}_m^T. \quad (8)$$

Because the ensemble perturbation matrix $\mathbf{X}_m$ only pertains to model variables within the spatially local influence volume associated with x_m, we refer to the ensemble based TLMs in either (7) or (8) as Local Ensemble TLMs or LETLMs for short.

To propagate a perturbation of the entire state vector one time step, one simply performs the embarrassingly scalable operation of time stepping each local variable by applying its own

This article is protected by copyright. All rights reserved.

LETLM to the perturbation variables within its influence volume. To propagate a second time step, one simply repeats all the operations from the first time step but this time using the ensemble perturbations relevant to this later time. Since the ensemble would typically have been run over the entire data assimilation window before the LETLM was run, one could, in principle, pre-compute the LETLMs for every time step across the data assimilation window. Such an approach would result in fast, scalable computer code. For the examples shown in this paper, we did not do this, we computed the LETLMs from the ensemble forecast when and as needed.

If the amplitudes of the ensemble perturbations are too large to ignore non-linear terms in the model Taylor expansion, then (7) and (8) will not give the true TLM. However, in this case, one may replace (6) by the approximation

$$\Xi_m = \mathbf{M}_m^{\mathrm{BLUE}}\left(i+1,i\right)\mathbf{X}_m + \zeta \tag{9}$$

where ζ is a random matrix giving the errors of the linear predictions $\mathbf{M}_m^{\mathrm{BLUE}}\mathbf{X}_m$ of the elements of the row vector Ξ_m. Provided that the error matrix ζ has an expected value of zero over many independent trials and that they are independent of the initial ensemble perturbations so that $\left\langle \zeta \mathbf{X}^T \right\rangle = \mathbf{0}$ then one can show that

$$\mathbf{M}_m^{\mathrm{BLUE}}\left(i+1,i\right) = \left\langle \Xi_m \mathbf{X}_m^T \right\rangle \left\langle \mathbf{X}_m \mathbf{X}_m^T \right\rangle^{-1}. \tag{10}$$

Author Manuscript

This article is protected by copyright. All rights reserved.

where the angle brackets indicate the average over an infinite number of independent trials (i.e. the expectation operator). Lorence and Payne (2007) refer to $\mathbf{M}_m^{\mathrm{BLUE}}$ as a *statistical* TLM. The estimates given by $\mathbf{M}_m^{\mathrm{BLUE}}\mathbf{X}_m$ are also sometimes referred to as the Best Linear Unbiased Estimates (BLUE).

Since in the limit of an infinitely large number of ensemble members $\left\langle \frac{\mathbf{X}_m\mathbf{X}_m^T}{K-1} \right\rangle = \frac{\mathbf{X}_m\mathbf{X}_m^T}{K-1}$ and $\left\langle \frac{\Xi_m\mathbf{X}_m^T}{K-1} \right\rangle = \frac{\Xi_m\mathbf{X}_m^T}{K-1}$ it follows that the $\mathbf{M}_m$ defined by equation (7) satisfies

$$\text{As } K \to \infty,\ \mathbf{M}_m = \mathbf{M}_m^{\mathrm{BLUE}} \tag{11}$$

and hence with finite K the $\mathbf{M}_m$ given by (7) is an unbiased estimate of the statistical TLM $\mathbf{M}_m^{\mathrm{BLUE}}$.

In the non-linear regime, the LETLM given by (8) also has a noteworthy property. Specifically, for *any* arbitrary initial perturbation $\mathbf{x}'_m$ that can be represented as a linear sum of ensemble perturbations so that $\mathbf{x}'_m = \mathbf{X}_m\mathbf{b}$ where $\mathbf{b}$ is a vector whose i^{th} element gives the coefficient of the i^{th} column/perturbation of $\mathbf{X}_m$, then

$$\Xi_m\left(\mathbf{X}_m^T\mathbf{X}_m\right)^{-1}\mathbf{X}_m^T\mathbf{x}'_m = \mathbf{M}_m\mathbf{X}_m\mathbf{b} = \Xi_m\left(\mathbf{X}_m^T\mathbf{X}_m\right)^{-1}\mathbf{X}_m^T\mathbf{X}_m\mathbf{b} = \Xi_m\mathbf{b}. \tag{12}$$

Hence, in this special case, equation (8) represents the evolution of perturbations obtained by simply holding the coefficients of the ensemble perturbations constant through time.

Author Manuscript

This article is protected by copyright. All rights reserved.

Equations (11) and (12) apply even if the ensemble perturbations do not satisfy a strictly linear set of equations either because their amplitude is too large or because the system is formally non-differentiable and hence impossible to linearize. They suggest that the LETLM delivers a reasonable linear approximation to the evolution of non-linear perturbations.

4. LETLM for simple coupled model

4.1 Construction of LETLM

We begin by defining the influence regions for each model variable. Ideally, the influence region should be big enough to contain all the variables that influence the evolution of the variable of interest over the time step of interest and small enough to allow the ensemble sub-space to span the vector space of possible linear evolutions.

The abscissa axes of the simple model shown in Figure 1 indicate the horizontal indices of the model variables at the four levels of our simple model. For the sake of discussion, we shall assume that the variables on the left side of the page are in the West and those on the right side of the page are in the East so that variables with larger indices lie to the East of variables with smaller indices.

Equation (A1) from the Appendix suggests that the evolution of a variable over a single time-step would only depend on the closest two variables on its Western side and the closest variable on its Eastern side. However, since we employed 2nd order Runge-Kutta time stepping that includes one intermediate time step, the evolution has non-zero sensitivity to the 3rd and 4th

Author Manuscript

This article is protected by copyright. All rights reserved.

closest variables on its Western side and to the 2nd closest variable on its Eastern side. Hence, by numerical design the evolution only has sensitivity to the 4 variables on its West, itself and two variables on its East. That's 7 variables in total. For simplicity (and also since the asymmetry in the horizontal differencing in this model is unusual) we assume an LETLM horizontal influence region that includes four variables to both the East and West of the variable to be updated: Nine contiguous grid-points in total centered on the variable to be updated

Examination of (A2) from the Appendix shows that the evolution of each element of the upper atmospheric vector $\mathbf{a}_u$ depends only on corresponding elements of the atmospheric mixed layer vector $\mathbf{a}_l$. For this reason, the entire influence region for a variable in the upper atmospheric layer consists solely of the 9 contiguous grid points at its own level and the 9 contiguous grid points in the layer immediately beneath it: 18 variables in total.

The second line of equation (A2) shows that elements of the atmospheric boundary layer vector $\mathbf{a}_l$ are influenced by corresponding elements of the 5-grid-point averages of oceanic-boundary-layer-variables $\mathbf{o}_u$ given by $\mathbf{L}\mathbf{o}_u$ and corresponding elements of the upper atmosphere vector $\mathbf{a}_u$. Hence, the influence region for variables in the atmospheric boundary layer was chosen to consist of the nine 5-grid-point averages of the oceanic boundary layer variables corresponding to the nine grid points of the atmospheric boundary layer influence region, plus the vertically aligned 9 grid points in both the atmospheric boundary layer and the upper

Author Manuscript

This article is protected by copyright. All rights reserved.

atmosphere. Thus, the influence region for an atmospheric boundary layer variable contains 27 variables.

For similar reasons, the influence region for a variable in the oceanic mixed layer was also defined to contain 27 variables: 9 variables at its own level, 9 vertically aligned variables from the deeper ocean level and the 9 contiguous variables from the atmospheric boundary layer whose central point over-laps with the variable being updated in the oceanic mixed layer. Finally, the influence region for variables in the deepest ocean layer contains 18 variables: 9 variables at its own level and 9 vertically aligned variables from the oceanic mixed layer.

Having defined the influence region for each coupled model variable, it is useful to consider the types of perturbations that will need to be propagated by the TLM. Do these perturbations lie on some sub-space of the complete vector-space of the influence volume? If so, is it possible to construct an ensemble generation method that will accurately sample this sub-space? How many ensemble members would be required to span this sub-space?

Here we consider the case where the LETLM will be required to accurately propagate *any* initial test perturbation $\delta\mathbf{x}_0^{test}$ where the elements of $\delta\mathbf{x}_0^{test}$ are random normal uncorrelated variables with a mean of zero. One obtains the non-linear evolution of $\delta\mathbf{x}_0^{test}$ through time by using the non-linear model to (i) propagate the perturbed initial condition $\mathbf{x}_0^{test} = \mathbf{x}_0^{g} + \delta\mathbf{x}_0^{test}$ (ii) propagate the unperturbed initial condition $\mathbf{x}_0^{g}$, and (iii) subtracting the propagated state obtained from (ii) from that obtained from (i). For the TLM and adjoint tests discussed in Section 4 and 5

Author Manuscript

This article is protected by copyright. All rights reserved.

of this paper, we chose $\mathbf{x}_0^g$ to be the mean of the 480 member climatological ensemble shown on Figure 1. We output both the perturbed and unperturbed non-linear trajectories every 6 hrs out to 120 hrs (5 days) to obtain the vectors

$$\mathbf{x}_{6:120}^{test} = \begin{bmatrix} \mathbf{x}_6^{test} \\ \mathbf{x}_{12}^{test} \\ \vdots \\ \mathbf{x}_{120}^{test} \end{bmatrix}, \mathbf{x}_{6:120}^{g} = \begin{bmatrix} \mathbf{x}_6^{g} \\ \mathbf{x}_{12}^{g} \\ \vdots \\ \mathbf{x}_{120}^{g} \end{bmatrix}, \text{ and } \delta\mathbf{x}_{6:120}^{test} = \mathbf{x}_{6:120}^{test} - \mathbf{x}_{6:120}^{g}. \quad (13)$$

Provided the initial test perturbation $\delta\mathbf{x}_0^{test}$ is small enough the perturbation evolution described by the perturbation vector $\delta\mathbf{x}_{6:120}^{test}$ will be perfectly described by the true TLM. In our system, it was found that $\delta\mathbf{x}_{6:120}^{test}$ obeyed strictly linear dynamics when the random draws used to create $\delta\mathbf{x}_0^{test}$ had the variance 10^{-6}. In other words, when

$$\delta\mathbf{x}_0^{test} \sim N\left(\mathbf{0}, \frac{1}{10^6}\mathbf{I}\right), \quad (14)$$

$\delta\mathbf{x}_{6:120}^{test}$ obeyed linear dynamics. Note that such perturbations will be roughly four orders of magnitude smaller than the climatological range of coupled model values depicted in Figure 1.

For simplicity and to ensure that the ensemble sub-space would span the entire model vector sub-space in the limit of an infinite ensemble, we chose our *K* initial ensemble members to be given by $\mathbf{x}_0^i, i = 1, 2, ..., K$ where

Author Manuscript

This article is protected by copyright. All rights reserved.

$$\mathbf{x}_0^i = \mathbf{x}_0^g + \delta\mathbf{x}_0^i,\ i = 1,2,...,K \text{ where } \delta\mathbf{x}_0^i \sim N\left(\mathbf{0}, \frac{1}{10^6}\mathbf{I}\right) \quad (15)$$

In other words, the elements of the initial ensemble perturbations are random normally distributed numbers with mean zero and a variance of 10^{-6}. Thus, they are assumed to be drawn from exactly the same distribution as the test perturbation that the LETLM will be required to propagate. The ensemble perturbations are, however, entirely independent of the test perturbation. Because, in this case, the ensemble perturbations are very small, the contribution of the non-linear terms to their evolution will be negligible and hence, the propagation of these perturbations through time by the non-linear model will be equivalent to the true TLM. For this reason, we can hope to construct an LETLM that is *identical* to the true TLM. To test the sensitivity of the accuracy of the LETLM to the amplitude of the test and ensemble perturbations, we also tested cases in which they were drawn from distributions with higher amplitudes and lower amplitudes.

As previously discussed, for our idealized coupled model, some of the influence regions have 18 variables, others have 27. In this case, 18 and 27 linearly independent small amplitude ensemble perturbations are sufficient to precisely define the true TLM in the influence regions that have 18 and 27 variables, respectively. It was found that just K=28 ensemble perturbations initialized using (13) were required to produce the required level of linear independence.

4.2 Test of LETLM

Author Manuscript

This article is protected by copyright. All rights reserved.

The influence volumes described in the previous subsection were used to construct the LETLMs described in Section 3 for each coupled model variable. Each LETLM was based on the 28 member ensemble initialized by (15) and propagated through time out to 120 hrs. To construct the LETLM for each 6 hr time step of the non-linear model, the ensemble was written out every 6 hrs. The initial test perturbation $\delta\mathbf{x}_0^{test}$ was then propagated through time, one 6 hr time step after the other, using the LETLM defined by equation (7). We denote the perturbation trajectory that resulted from these operations $\delta\mathbf{x}_{6:120}^{LETLM}$ where

$$\delta\mathbf{x}_{6:120}^{LETLM} = \begin{bmatrix} \delta\mathbf{x}_6^{LETLM} \\ \delta\mathbf{x}_{12}^{LETLM} \\ \vdots \\ \delta\mathbf{x}_{120}^{LETLM} \end{bmatrix}. \quad (16)$$

Figure 4 shows that the 5 day prediction $\delta\mathbf{x}_{120}^{LETLM}$ (red-line) is almost identical to $\delta\mathbf{x}_{120}^{test} = \mathbf{x}_{120}^{test} - \mathbf{x}_{120}^{g}$ (black line). Because the LETLM is so accurate, the black line is almost entirely obscured by the red line. The thin blue line gives the very poor prediction of the black line that would be obtained if the influence volume covered the entire model domain; i.e. it is the prediction obtained with no localization and only 28 ensemble members. The thick cyan line gives the very accurate prediction of the black line from an ETLM that uses an ensemble so large (480 members) that no localization is necessary.

To provide an overall measure of the accuracy of the TLM, we computed the normalized root mean square error of the LETLM using

Author Manuscript

This article is protected by copyright. All rights reserved.

$$nrmse\left(LETLM\right)=\sqrt{\frac{\left(\delta\mathbf{x}_{6:120}^{LETLM}-\delta\mathbf{x}_{6:120}^{test}\right)^{T}\left(\delta\mathbf{x}_{6:120}^{LETLM}-\delta\mathbf{x}_{6:120}^{test}\right)}{\left(\delta\mathbf{x}_{6:120}^{test}\right)^{T}\left(\delta\mathbf{x}_{6:120}^{test}\right)}}. \quad (17)$$

For the case depicted in Figure 4, $nrmse\left(LETLM\right)=3x10^{-4}$. The experiment was repeated for different random seeds and in all cases examined $nrmse\left(LETLM\right)<10^{-3}$. Furthermore, when figures like figure 4 were examined at each output time, it was invariably extremely difficult visually distinguish between $\delta\mathbf{x}_t^{LETLM}$ from $\delta\mathbf{x}_t^{test}$. These results are consistent with the mathematical analysis of Section 3 showing that LETLMs can be just as accurate as true TLMs provided the ensemble perturbations are in the linear regime.

To test the dependence of this accuracy to the amplitude of the ensemble and test perturbations, we assigned different variances to the distributions from which the perturbations were drawn and repeated the test. For variances of 10^{-2}, 10^{-4} and 10^{-12}, we found that the $nrmse\left(LETLM\right)$ was equal to 315, $187x10^{-4}$ and $2.5x10^{-4}$, respectively. Thus, large discrepancies only occurred in the case where the initial perturbations were given the relatively large variance of 10^{-2}. The linearity assumption was the least justified in this case – particularly in the later stages of the 5 day integration where the perturbations became quite large. Note that for perturbations with variances of 10^{-6} and 10^{-12} the *nrmses* were quite similar at $3x10^{-4}$ and $2.5x10^{-4}$, respectively, and hence do not appear to be converging to zero. We hypothesize that this apparent lower bound on error is due to a simplifying assumption we made when choosing

Author Manuscript

This article is protected by copyright. All rights reserved.

LETLM predictors for the atmospheric boundary layer. Specifically, we used spatial averages of the oceanic boundary layer as predictors rather than raw oceanic boundary layer variables because the ocean-atmosphere coupler only allowed the coarser resolution atmosphere to feel averages of the ocean model variables. However, our use of Runge-Kutta time-stepping means that the spatial averages of ocean variables at two distinct times contribute to changes in atmospheric boundary layer variables. The difference between the spatial averages at the two distinct times depends on the full resolution ocean state and hence there is a small but irreducible error associated with our decision to use spatial averages of the ocean variables as predictors of the atmospheric boundary layer variables. Nevertheless, as demonstrated from both equation (17) and Figure 4, this error remains extremely small over a 5 day window.

5. Adjoint of the LETLM

Errico and Vukicevic (1992) and Rabier et al. (1996), amongst others, demonstrated how the transpose or adjoint of the TLM can be used to give the gradient of some aspect of the forecast to a change in the initial conditions. Here, we demonstrate the extreme simplicity of deriving the adjoint of an LETLM and then use the adjoint of the LETLM to demonstrate how the sensitivity of forecasts to changes in the initial conditions critically depends on the forecast lead time.

5.1 Construction of the adjoint of the LETLM

Author Manuscript

This article is protected by copyright. All rights reserved.

Let $\mathbf{S}_m$ be the matrix that maps the global state L-vector $\mathbf{x}$ to the list of variables in the n-vector $\mathbf{x}_m$ defining the influence volume required to evolve the m^{th} model variable over a single time step so that

$$\mathbf{x}_m = \mathbf{S}_m \mathbf{x} \tag{18}$$

$\mathbf{S}_m$ has as many rows as there are variables in the m^{th} influence volume and as many columns as there are variables in the global state vector. There is only one element in each row of $\mathbf{S}_m$ that is not equal to zero and this element is equal to unity (one). Let the index j be the index of the column of the i^{th} row of $\mathbf{S}_m$ that is equal to unity; then the i^{th} row maps the j^{th} element of the vector $\mathbf{x}$ to the i^{th} element of the local vector $\mathbf{x}_m$. Hence, the j^{th} row of $\mathbf{S}_m^T$ in the operation $\mathbf{S}_m^T \mathbf{x}_m$ maps the i^{th} element of the local vector $\mathbf{x}_m$ back to the row of the global state vector from which it originally came. Hence, the operation $\mathbf{S}_m^T \mathbf{x}_m$ simply puts all of the variables in $\mathbf{x}_m$ onto the positions in the global state vector to which they originally belonged. Hence, to apply the adjoint of the LETLM to an arbitrary global L-vector $\mathbf{z}$ with elements $\mathbf{z}^T = \left[z_1, z_2, ..., z_m, ..., z_L \right]$, one uses

$$\mathbf{M}\left(i+1,i\right)^T \mathbf{z} = \sum_{m=1}^{L} \mathbf{S}_m^T \mathbf{M}_m \left(i+1,i\right)^T z_m \tag{19}$$

Where $\mathbf{M}\left(i+1,i\right)^T$ denotes the adjoint of the global TLM implied by the complete set of LETLMs, $\left\{ \mathbf{M}_1, \mathbf{M}_2, ..., \mathbf{M}_m, ..., \mathbf{M}_L \right\}$ that are defined by equation (7). Recall that, according to

Author Manuscript

This article is protected by copyright. All rights reserved.

(7), each LETLM is a local row vector and hence the $\mathbf{M}_m\left(i+1,i\right)^T$ in (19) is a local column vector. Note also that *L-n* of the rows in $\mathbf{S}_m^T$ are entirely filled with zeros. Hence, in practice, one only has to consider the effect of the *n*-rows of $\mathbf{S}_m^T$ that are non-zero and hence the operation $\mathbf{S}_m^T\mathbf{M}_m^T$ is extremely rapid because it amounts to simply assigning the correct global index to the *n*-variables listed in the local influence vector $\mathbf{M}_m^T z_m$.

Eq. (19) is a trivial rearrangement of the LETLM and hence code for the adjoint of an LETLM is readily obtained from the LETLM code.

A simple but effective test for computer code designed to represent the adjoint or transpose of a TLM is to recognize that the transpose of a scalar is equal to the original scalar and hence

$$0=\left|\left(\mathbf{z}^T\mathbf{M}^T\mathbf{z}\right)-\left(\mathbf{z}^T\mathbf{M}^T\mathbf{z}\right)^T\right|=\left|\mathbf{z}^T\left(\mathbf{M}^T\mathbf{z}\right)-\mathbf{z}^T\left(\mathbf{M}\mathbf{z}\right)\right| \qquad (20)$$

where $\mathbf{z}$ is *any* random vector with appropriate length. Hence, to test the code for the adjoint of any $\mathbf{M}$ over any time interval, one can compute $\mathbf{M}^T\mathbf{z}$ and $\mathbf{M}\mathbf{z}$ and then use the resulting vectors in the right hand side of (20). If the adjoint computer code has been correctly implemented, the result of (20) will be as close to zero as permitted by the precision of the floating point operations of the computer. Eq (20) was used to confirm the correctness of the adjoint code for all of the adjoint time intervals discussed in this paper.

5.2 Using the adjoint of the LETLM to compute forecast sensitivity

Author Manuscript

This article is protected by copyright. All rights reserved.

For simplicity, here we just consider the sensitivity of the gradient of a single model forecast variable to changes in the state vector at an earlier time. From this sensitivity, it is straightforward to compute the sensitivity of *any* scalar function of the model forecast variables.

Let $\mathbf{M}(i+J,i) = \mathbf{M}\left(i+J,i+J-1\right),...,\mathbf{M}\left(i+2,i+1\right)\mathbf{M}\left(i+1,i\right)$ denote the global TLM that maps a perturbation $\delta\mathbf{x}$ from the i^{th} time step to the $(i+J)^{\text{th}}$ time step. Let $\mathbf{e}_m^T$ be the unit vector that selects the m^{th} element of the global state vector, then we can write

$$\delta x_m\left[\left(i+J\right)\delta t\right] = \mathbf{e}_m^T\mathbf{M}(i+J,i)\left(\delta\mathbf{x}\right) = \sum_{l=1}^{L}\mu_{ml}\left(\delta x_l\right), \tag{21}$$

where μ_{ml} is equal to the inner product of $\mathbf{e}_m$ with the l^{th} column of $\mathbf{M}(i+J,i)$. The derivative, gradient or sensitivity of the state of the m^{th} variable $\delta x_m\left[\left(i+J\right)\delta t\right]$ at the $\left(i+J\right)^{\text{th}}$ time step with respect to changes in the perturbation at the i^{th} time step is then given by

$$\begin{aligned}\frac{\partial\left\{\delta x_m\left[\left(i+J\right)\delta t\right]\right\}}{\partial\left(\delta\mathbf{x}\right)} &= \begin{bmatrix}\dfrac{\partial\left\{\delta x_m\left[\left(i+J\right)\delta t\right]\right\}}{\partial\left(\delta x_{m1}\right)}\\ \dfrac{\partial\left\{\delta x_m\left[\left(i+J\right)\delta t\right]\right\}}{\partial\left(\delta x_{m2}\right)}\\ \vdots\\ \dfrac{\partial\left\{\delta x_m\left[\left(i+J\right)\delta t\right]\right\}}{\partial\left(\delta x_{mL}\right)}\end{bmatrix} = \begin{bmatrix}\mu_{m1}\\ \mu_{m2}\\ \vdots\\ \mu_{mL}\end{bmatrix}\\ &= \mathbf{M}(i+J,i)^T\mathbf{e}_m = \mathbf{M}\left(i+1,i\right)^T\mathbf{M}\left(i+2,i+1\right)^T...\,\mathbf{M}\left(i+J,i+J-1\right)^T\mathbf{e}_m\end{aligned} \tag{22}$$

Author Manuscript

This article is protected by copyright. All rights reserved.

Thus, the vector describing the change in $\left\{\delta x_m\left[\left(i+J\right)\delta t\right]\right\}$ at the $\left(i+J\right)^{\text{th}}$ time step engendered by changes in each of the variables comprising a perturbation vector $\delta\mathbf{x}$ at the earlier i^{th} time step is given by integrating the unit vector $\mathbf{e}_m$ backward in time using the adjoint of the TLM. Equations (22) and (19) allow us to perform this reverse time adjoint integration using LETLMs.

To illustrate the fascinating perspective on development in coupled model systems that would be enabled by the LETLMs and their adjoints, we used (22) and (19) to compute the sensitivity of forecasts of the 50th variable in the oceanic boundary layer to changes in the state at earlier times. We shall call this 50th variable the *verification* variable.

The solid line on Figure 5 gives the computed sensitivity of the 12 hr forecast of the 50th variable in the oceanic boundary layer to infinitesimal changes in the initial condition. At this time, the greatest sensitivity is to changes in the oceanic boundary layer near the 50th grid point. The second largest sensitivity is to changes to the atmospheric boundary layer variables lying to the West of the verification variable.

The feasibility of a LETLM for a 12 hr time step, rather than the 6 hr time step, is indicated by the fact that the region of sensitivity over this 12 hr forecast period is still closely localized around the verification point. Provided one ensured that (i) the influence volume for the verification point included all of the variables with non-negligible sensitivity over the 12 hr period and (ii) that the ensemble contained more linearly independent perturbations than the number of variables in the influence volume, the accuracy of such a 12 hr LETLM would be guaranteed. Because the influence volume is larger for a 12 hr time step than a 6 hr time step, the

Author Manuscript

This article is protected by copyright. All rights reserved.

LETLM ensemble size for a 12 hr time step would need to be correspondingly larger than that for the 6 hr time step. Thus, Figure 5 shows how the adjoint associated with a small time step (6 hrs in this case) could be used to help determine the required size of the influence volume and corresponding ensemble size for a larger time step (12 hrs in this case).

Figure 6 gives the computed sensitivity of the 5 day forecast of the 50^{th} variable in the oceanic boundary layer to infinitesimal changes in the initial conditions. At this time, the greatest sensitivities are to atmospheric boundary and upper layer variables lying to the West of the verification variable. This means that the correction of small errors in the atmospheric boundary layer would be more effective at correcting errors in the 5 day forecast of the oceanic boundary layer verification variable than correcting variables in the oceanic boundary layer by a similar amount.

To summarize: (i) the adjoint of an LETLM is trivial to derive from the LETLM (ii) the adjoint is a powerful tool for understanding model dynamics and designing observational networks, and (iii) the adjoint of an LETLM with relatively short time steps can be used to guide the development of adjoints with significantly longer time steps.

6. Demonstration of the use of LETLMs in strong constraint 4DVAR

A compelling reason for developing TLMs and their adjoints is that they enable one to find a model trajectory like $\left(\mathbf{x}_{0:120}\right)^T = \left[\mathbf{x}_0, \mathbf{x}_6, \ldots, \mathbf{x}_{120}\right]$ that would minimize a penalty function like

Author Manuscript

This article is protected by copyright. All rights reserved.

$$
\begin{aligned}
&J\left(\mathbf{x}_{0:120}\right) = J_b\left(\mathbf{x}_{0:120}\right) + J_o\left(\mathbf{x}_{0:120}\right), \text{ where} \\
&J_b\left(\mathbf{x}_{0:120}\right) = \frac{1}{2}\left(\mathbf{x}_0^f - \mathbf{x}_0\right)^T \mathbf{P}_0^{f-1}\left(\mathbf{x}_0^f - \mathbf{x}_0\right), \qquad (23) \\
&J_o\left(\mathbf{x}_{0:120}\right) = \frac{1}{2}\left[\mathbf{y}_{0:120} - H\left(\mathbf{x}_{0:120}\right)\right]^T \mathbf{R}^{-1}\left[\mathbf{y}_{0:120} - H\left(\mathbf{x}_{0:120}\right)\right]
\end{aligned}
$$

In (23) the symbols $\mathbf{x}_0^f$, $\mathbf{P}_0^f$, $\mathbf{y}_{0:120}$, $H\left(\mathbf{x}_{0:120}\right)$ and $\mathbf{R}$ respectively refer to the prior mean or first guess, the first guess error covariance matrix, the vector of observations and the estimate of these observations from the state $\mathbf{x}_{0:120}$ using the observation operator *H*. Assuming that $\mathbf{x}_0^f$ and $\mathbf{y}_{0:120}$ are unbiased with Gaussian error statistics then for a model with no model error, the initial state $\mathbf{x}_0$ that minimizes (23) is a mode of the posterior distribution of truth given the assimilated observations. Here, we demonstrate the use of LETLMs in strong constraint 4DVAR by using them to minimize (23) for the special case where $\mathbf{y}_{0:120}$ was obtained by taking 5 equally spaced observations at each model level every 6 hrs over a 120 hr data assimilation window. Note that this 120 hr data assimilation window considered here is much longer than the 6 hr time step to be used for the LETLM. The prior mean $\mathbf{x}_0^f$ and covariance $\mathbf{P}_0^f$ in (23) were taken to be the mean and covariance of 480 members of the first set of climatological samples discussed earlier while the initial truth was taken to be a random selection from the second set of 500 random climatological samples discussed earlier. This approach ensures that the initial truth is not a member of the sample used to construct the initial mean and covariance. The observations were always equally spaced in the horizontal but their locations would randomly vary from one 6 hr period to the next. The observations were given an observation error covariance of **R** by adding a

Author Manuscript

This article is protected by copyright. All rights reserved.

random vector with mean zero and covariance $\mathbf{R}$ to the truth. The matrix $\mathbf{R}$ was assumed to be diagonal with all diagonal elements assigned a value of 0.25 $\left(\mathbf{R} = 0.25\mathbf{I}\right)$. This chosen observation error variance of ¼ ensures that each observation contains information about the true state that is much greater than that contained within climatology. Quantitatively, the variance ¼ corresponds to a standard deviation of ½ which is slightly greater than one tenth of the domain averaged climatological standard deviation of 4.1.

As discussed in Tremolet (2007), for example, 4DVAR outer loops are required to find the minimum of (23) when the errors are affected by non-linear dynamics. In our case, the errors are strongly affected by non-linear dynamics because the first guess and its covariance were taken from climatology. Tremolet (2007) noted that inconsistencies between the TLM and the non-linear model could prevent the outer loop from converging. Since the LETLM and its adjoint are perfectly consistent with the non-linear model, no such inconsistencies are present in our implementation and, as shown in Figure 7, the outer loop reduced the mean square error (mse) of the state estimate by more than an order of magnitude over 6 outer loop iterations. Figure 7 also shows that outer loop iterations 7 through 10 failed to produce any significant further reduction in mse. The large mse reductions from outer loop iterations 1 through 6 are, presumably, associated with the facts that (i) by construction, the error of the climatological mean used as the first guess is governed by highly non-linear dynamics, and (ii) there are enough observations over the 5 day window to cause the mode of the posterior distribution to lie close to the truth.

Author Manuscript

This article is protected by copyright. All rights reserved.

To visualize just how close the trajectory obtained from these iterations is to the the truth and the assimilated observations, snapshots of these entities are compared in Figures 8, 9 and 10. The figures show that the algorithm has arrived at a trajectory that tracks the truth closely in the atmosphere and fairly closely in the ocean over the entire 5 day period. It is unsurprising that the analysis is more accurate in the atmosphere than the ocean because the distance between observations is similar to the length scale of atmospheric perturbations while being much larger than the length scale of perturbations in the ocean. The profound reduction in error depicted in Figure 7 shows that the strong constraint of the non-linear dynamical model imposed by LETLM enabled 4DVAR is extremely effective at reducing state estimation error in this case.

To help visualize *how* the 4DVAR is able to find an initial condition that leads to a forecast that can track the observations over 5 days with such a sparse spatio-temporal distribution of observations, consider the left panels of Figure 11. They depict the LETLM forecast error correlation between all of the initial time variables and the 50^{th} oceanic model variable at day 5. They show that errors in the 5 day forecast of an oceanic boundary layer variable have significant correlations with errors over wide regions in the oceanic boundary layer, the atmospheric boundary layer and, to a lesser extent, the upper atmosphere. This shows how 4DVAR can use observations of the oceanic boundary layer at day 5 to improve the state estimate at day 0.

Also note that this correlation function is very closely related to the adjoint sensitivity shown in Fig. 6. Specifically, the covariance function corresponding to the left panels in Fig. 11 can be

Author Manuscript

This article is protected by copyright. All rights reserved.

obtained by left multiplying the adjoint sensitivity vector shown in Fig. 6 by the initial climatological covariance matrix. Note that the error correlation function shows large amplitude variations in the oceanic boundary layer whereas such variations are largely absent from the adjoint sensitivity function (Fig. 6). Fig. 12 shows that the initial time atmospheric boundary layer errors are, in fact, strongly correlated with oceanic boundary layer errors. Hence, the large amplitude variations of error correlations in the oceanic boundary layer are due to the fact that initial errors in the atmospheric boundary layer are strongly correlated with those in the oceanic boundary layer (Figure 12). In this way, the error correlation function on the left side of Figure 11 can be seen to combine dynamical adjoint sensitivity information with initial forecast error covariance information.

As noted in Hodyss et al. (2016), a key difference between four-dimensional data assimilation schemes that use TLM/adjoints such as 4DVAR and those that do not such as Ensemble Kalman Smoothers and 4DEnVARs pertains to the type of four-dimensional error covariance models used by the schemes. In 4DVAR, the four dimensional error covariance matrix is generated by propagating the initial covariance matrix through time using a linear model; whereas in the 4D schemes that do not use TLMs and adjoints, it is propagated through time using a non-linear model. Hence, in considering methods for coupled data assimilation, it is of interest to compare and contrast 4D error correlation functions obtained with linear and non-linear models.

Author Manuscript

This article is protected by copyright. All rights reserved.

The 4D correlation function on the left side of Figure 11 was obtained by propagating 480 initial ensemble perturbations across the 5 day window using the LETLM. The correlation function on the right side of Figure 11 was obtained in exactly the same way except that here the initial ensemble was propagated across the 5 day window using the *non-linear* model. Hence, the differences that can be seen between the left and right panels of Figure 11 are entirely due to the effect of non-linear terms on perturbation evolution. The shape of the correlation function on the right side of Figure 11 is broadly similar to that on the left but its amplitude is generally smaller. The amplitude difference is particularly marked near the location of the observation in the oceanic boundary layer and also in the upper atmosphere. We tentatively suggest that the higher amplitude of the 4D correlations produced by the TLM/adjoint relative to those produced by the ensemble might, in general, enable 4DVAR to obtain more accurate analyses over long data assimilation windows than 4DVAR schemes that do not use the TLM/adjoint.

Conclusions

The demand for advanced data assimilation in coupled models is driven by the belief that it will ultimately deliver the best estimates of the coupled model state and its evolution. Coupled models offer our best chance for long range environmental forecasting. Relative to atmosphere-only or ocean-only forecast models, the current and planned coupled ocean, wave, ice, atmosphere and aerosol models represent a quantum leap in complexity. Building and maintaining accurate traditional TLM and adjoints for these systems is a daunting prospect. However, since ensembles are a cornerstone of any long range forecasting capability, coupled

Author Manuscript

This article is protected by copyright. All rights reserved.

model ensembles are readily available and, by construction, keep pace with the ever evolving components of coupled models. Here, we have used an idealized coupled model to demonstrate the following:

(i) Local Ensemble TLMs (LETLMs) of coupled models and their adjoints are easy to construct and can be precisely accurate provided the ensemble size exceeds the maximum number of independent variables that influence the evolution of model variables over a time step.

(ii) Adjoints of LETLMs provide an extremely powerful tool for studying and understanding coupled model dynamics, and

(iii) LETLMs and their adjoints can be used in 4DVAR data assimilation schemes.

In some models, the number of *independent* variables that influence evolution will be smaller than the total number of variables within an influence volume and hence, in such cases, accurate LETLMs will be achievable with fewer ensemble members than the number of variables in the influence volume.

In the simple coupled model considered in this paper the time step of the oceanic and atmospheric models was the same. In the sophisticated coupled models used to make real world predictions the time steps of sub-components can differ. Nevertheless, it should be straightforward to create LETLMs for each subcomponent and the couplers between each subcomponent using the general approach outlined here.

Author Manuscript

This article is protected by copyright. All rights reserved.

Much work remains to optimize LETLM computational efficiency. Should one integrate the LETLM using small time steps and a relatively small ensemble or should one use larger time steps with a larger ensemble? To minimize the cost of input-output operations, could one build and then store in memory all of the LETLMs needed to propagate each model variable across the entire data assimilation window? (Recall that the adjoint of the LETLM is trivially obtainable from the LETLM). Doing so would make runs of the LETLM forward in time and its adjoint backward in time extremely scalable for the multiple forward and backward sweeps required by typical 4DVAR minimization algorithms. Future work will address these issues and test them in significantly more realistic models than that used here.

Appendix: Detailed description of coupled model

The evolution of each variable in the coupled model is determined via two distinct computational steps. For the first step, at each vertical level, Lorenz's (2005) model 1 equation

$$\frac{dX_\beta}{dt} = a\left[-X_{\beta-2}X_{\beta-1} + X_{\beta-1}X_{\beta+1} - X_\beta + F\right] \tag{A1}$$

is integrated one time step using 2nd order Runge-Kutta time stepping. The integer subscript β defines the horizontal position of the model variable. The scalar forcing factor F was set equal to 11 for all vertical layers except for the deepest ocean layer where it was set equal to 22 because doing so increased the dynamical independence of this deepest ocean layer from the other layers.

Author Manuscript

This article is protected by copyright. All rights reserved.

The scalar factor a influences the time scale of evolution. We set a=1 in both atmospheric layers. We use a non-dimensional time step of 0.05. Lorenz (2005) points out that an analogy with the waves supported by (A1) and atmospheric Rossby waves suggests that a time step of 0.05 is "like" a time step of about 6 hrs. To force the "ocean" to evolve more slowly than the atmosphere, we set a=1/3 in both ocean layers.

Having integrated (A1) forward in time by one time step at each layer of the model, one obtains updated estimates of the vectors $\mathbf{a}_u, \mathbf{a}_l, \mathbf{o}_u$ and $\mathbf{o}_l$ where $\mathbf{a}_u$ lists the 20 variables of the upper atmosphere, $\mathbf{a}_l$ the 20 variables of the lower atmosphere, $\mathbf{o}_u$ the 100 variables of the upper ocean and $\mathbf{o}_l$ the 100 variables of the lower ocean. Vertical dynamic coupling between the updated estimates of $\mathbf{a}_u, \mathbf{a}_l, \mathbf{o}_u$ and $\mathbf{o}_l$ is then imposed by updating them again using the vertical coupling equations

$$\begin{aligned}
\mathbf{a}_u &= \mathbf{a}_u w_a + \mathbf{a}_l (1 - w_a), && \text{where } w_a = 0.99 \\
\mathbf{a}_l &= \mathbf{a}_l w_{al} + (\mathbf{L}\mathbf{o}_u) w_{ao} + \mathbf{a}_u (1 - w_{al} - w_{ao}), && \text{where } w_{al} = 0.85 \text{ and } w_{ao} = 0.14 \\
\mathbf{o}_u &= \mathbf{o}_u w_{ou} + (\mathbf{U}\mathbf{a}_l) w_{oa} + \mathbf{o}_l (1 - w_{al} - w_{ao}), && \text{where } w_{ou} = 0.85 \text{ and } w_{ao} = 0.12 \\
\mathbf{o}_l &= \mathbf{o}_l w_o + \mathbf{o}_u (1 - w_o), && \text{where } w_o = 0.97.
\end{aligned} \tag{A2}$$

In (A2), the matrix $\mathbf{L}$ is a 20x100 matrix that takes 5-grid-point averages of the oceanic mixed layer variables which ensures that each of the 20 atmospheric boundary layer variables is influenced by a single and unique average of 5 contiguous oceanic-mixed-layer-variables. Each row of $\mathbf{L}$ has 5 contiguous elements that are all equal to 1/5; all of the other elements in that row

Author Manuscript

This article is protected by copyright. All rights reserved.

of **L** are equal to zero. The matrix **U** is a 100x20 matrix that replicates and aligns each of the 20 atmospheric boundary layer variables with the 5 contiguous oceanic mixed layer variables whose average influences the replicated atmospheric boundary layer variable. Each column of **U** contains 5 contiguous elements that are all equal to one; all other column elements are equal to zero.

The values of the weights used and specified in (A2) were obtained via an interactive tuning process aimed at achieving the four quasi-realistic ocean-atmosphere features given in Section 2. The coupled model Matlab code is available upon request.

Acknowledgements: Craig H. Bishop and Sergey Frolov gratefully acknowledge financial support from the Office of Naval Research Grants # N0001413WX00008. David D. Kuhl acknowledges support from PMW-120 under Program Element 0603207N. David D. Kuhl and Karl Hoppel also acknowledge support from Office of Naval Research base funding via Task BE-435-050. Douglas R. Allen and Karl Hoppel acknowledge support from Office of Naval Research base funding via Task BE-033-02-42.

References

Anderson, J. L., 2001: An ensemble adjustment Kalman filter for data assimilation. *Mon. Wea. Rev.*, **129,** 2884–2903.

Anderson, J. L., 2003: A local least squares framework for ensemble filtering. *Mon. Wea.*

Author Manuscript

This article is protected by copyright. All rights reserved.

Rev., **131**, 634–642.

Bishop, C.H. and D. Hodyss, 2011: Adaptive ensemble covariance localization in ensemble 4D-VAR state estimation, *Mon. Wea . Rev.* **139,** 1241-1255.

Buehner, M., J. Morneau, C. Charette, 2013: Four-dimensional ensemble-variational data assimilation for global deterministic weather prediction. *Nonlin. Processes Geophys*., **20**, 669–682. doi:10.5194/npg-20-669-2013

Buizza R., and M. Leutbecher, 2015: The forecast skill horizon. *Q. J. Roy. Met. Soc.,* doi:10.1002/qj.2619

Chen, S., T. Cambell, H. Jin, S. Gabersek, R. Hodur, and P. Martin, 2010: Effect of Two-Way Air–Sea Coupling in High and Low Wind Speed Regimes. *Mon. Weather Rev.,* **138**, 3579–3602, doi:10.1175/2009MWR3119.1.

Clayton, A. M., Lorenc, A. C. and Barker, D. M. (2013), Operational implementation of a hybrid ensemble/4D-Var global data assimilation system at the Met Office. *Q.J.R. Meteorol. Soc.*, **139**: 1445–1461. doi: 10.1002/qj.2054

Courtier, P., Thépaut, J.-N. and Hollingsworth, A. (1994), A strategy for operational implementation of 4D-Var, using an incremental approach. *Q.J.R. Meteorol. Soc.*, **120**: 1367–1387.

Errico, R.M. and T. Vukicevic, 1992: Sensitivity Analysis Using an Adjoint of the PSU-NCAR Mesoseale Model. Mon. Wea. Rev., 120, 1644–1660.

Author Manuscript

This article is protected by copyright. All rights reserved.

Frolov, S. and C.H. Bishop, 2016: Ensemble-based tangent linear models and their use in propagating hybrid error covariance models. *Mon. Wea. Rev.* (In press).

Gauthier, P., M. Tanguay, S. Laroche, S. Pellerin, and J. Morneau, 2007: Extension of 3DVAR to 4DVAR: Implementation of 4DVAR at the Meteorological Service of Canada. *Mon. Wea. Rev.*, **135**, 2339–2354. doi: http://dx.doi.org/10.1175/MWR3394.1

Hodyss, D., C.H. Bishop and M. Morzfeld, 2016: The Differences between Ensemble and Variational Methods and Implications for their Fusion. *Mon. Wea. Rev.*

Hunt, B. R., E. J. Kostelich, and I. Szunyogh, 2007: Efficient Data Assimilation for Spatiotemporal Chaos *Phys. D*, **230**, 112–126. Local Ensemble Transform Kalm DOI:10.1016/j.physd.2006.11.008.

Julier, S.J., and J.K. Uhlmann, 2004: Unscented filtering and nonlinear estimation. *Proceedings of the IEEE,* **92**, 401 – 422. DOI:10.1109/JPROC.2003.823141

Kadowaki, Takashi. "A 4-dimensional variational assimilation system for the JMA Global Spectrum Model." CAS/JAC WGNE Research Activities in Atmospheric and Oceanic Modelling 34 (2005): 1-17.

Kuhl, D.D, T.E. Rosmond, C.H. Bishop, McLay, J.G., and Baker, N. L., 2013: Comparison of hybrid ensemble/4D-Var and 4D-Var within the NAVDAS-AR data assimilation framework. *Mon. Wea. Rev.,* **141**, 2740-2758.

Author Manuscript

This article is protected by copyright. All rights reserved.

Laloyaux, P., M. Balmaseda, D. Dee, K. Mogensen, and P. Janssen, 2015: A coupled DA system for climate reanalysis. *Q. J. Roy. Met. Soc.,* doi: 10.1002/qj.2629

Liu, C., Q. Xiao, and B. Wang, 2008: An ensemble-based four-dimensional variational data assimilation scheme. Part I: Technical formulation and preliminary test. *Mon. Wea. Rev.*, **136**, 3363–3373, doi:10.1175/2008MWR2312.1

Lorenc, A.C. and T. Payne, 2007: 4D-Var and the butterfly effect: Statistical four-dimensional data assimilation for a wide range of scales. *Q. J. R. Meteorol. Soc*., **133**, 607-614.

Lorenc, AC, NE Bowler, AM Clayton, SR Pring, and D Fairbairn, 2015: Comparison of Hybrid-4DEnVar and Hybrid-4DVar Data Assimilation Methods for Global NWP. *Mon. Wea. Rev.,* **143**, 212–229, doi: 10.1175/MWR-D-14-00195.1.

Lorenz, E. N., 2005: Designing Chaotic Models. *J. Atmos. Sci.,* **62**, 1574–1587.

MacLachlan, C., and Coauthors, 2014: Global Seasonal forecast system version 5 (GloSea5): a high-resolution seasonal forecast system. *Q. J. R. Meteorol. Soc.,* **140**, doi:10.1002/qj.2396. http://doi.wiley.com/10.1002/qj.2396

McGuffie, K., and A Henderson-Sellers, 2005: *A climate modelling primer*. *3rd Edition, John Wiley & Sons,* 275 pages. ISBN: 0-470-85751-X

Mulholland DP, Laloyaux P, Haines K, and MA Balmaseda, 2015: Origin and Impact of Initialization Shocks in Coupled Atmosphere–Ocean Forecasts. *Mon. Wea. Rev*., **143**, 4631–4644, doi: 10.1175/MWR-D-15-0076.1.

Author Manuscript

This article is protected by copyright. All rights reserved.

Rabier, F., Järvinen, H., Klinker, E., Mahfouf, J.-F. and Simmons, A., 2000: The ECMWF operational implementation of four-dimensional variational assimilation. I: Experimental results with simplified physics. *Q.J.R. Meteorol. Soc.*, **126**: 1143–1170.

Rabier, F., Klinker, E., Courtier, P. and Hollingsworth, A. (1996), Sensitivity of forecast errors to initial conditions. *Q.J.R. Meteorol. Soc*., 122: 121–150. doi:10.1002/qj.49712252906

Rawlins, F., Ballard, S. P., Bovis, K. J., Clayton, A. M., Li, D., Inverarity, G. W., Lorenc, A. C. and Payne, T. J., 2007: The Met Office global four-dimensional variational data assimilation scheme. *Q.J.R. Meteorol. Soc.*, 133: 347–362.

Rosmond, T. and Xu, L., 2006: Development of NAVDAS-AR: non-linear formulation and outer loop tests. *Tellus A*, **58**: 45–58. doi: 10.1111/j.1600-0870.2006.00148.x

Saha, S., and Coauthors, 2010: The NCEP climate forecast system reanalysis. *Bull. Am. Meteorol. Soc.,* **91**, 1015–1057, doi:10.1175/2010BAMS3001.1.

Shelly, A., P. Xavier, D. Copsey, T. Johns, J. M. Rodr, S. Milton, and N. Klingaman, 2014: Coupled versus uncoupled hindcast simulations of the Madden-Julian Oscillation in the Year of Tropical Convection. *Geophys. Res. Lett*., **41**, 5670–5677, doi:10.1002/2013GL059062.This.

Smith, P.J., Fowler, A.M. and Lawless, A.S., 2015: Exploring strategies for coupled 4D-Var data assimilation using an idealised atmosphere-ocean model. *Tellus A*, **67**, 27025, http://dx.doi.org/10.3402/tellusa.v67.27025.

Author Manuscript

This article is protected by copyright. All rights reserved.

Smith, T. A., and Coauthors, 2013: Ocean-wave coupled modeling in COAMPS-TC: A study of Hurricane Ivan (2004). *Ocean Model*., **69**, 181–194, doi:10.1016/j.ocemod.2013.06.003.

Tremolet, Y., 2007: Incremental 4D-Var convergence study. *Tellus A*, **59**: 706–718. doi: 10.1111/j.1600-0870.2007.00271.x

Xu, L., Rosmond, T. and Daley, R., 2005: Development of NAVDAS-AR: formulation and initial tests of the linear problem. Tellus A, 57: 546–559

Zhang S., M. J. Harrison, A. Rosati, and A. Wittenberg, 2007: System Design and Evaluation of Coupled Ensemble Data Assimilation for Global Oceanic Climate Studies. *Mon. Wea. Rev.*, **135**, 3541–3564.

doi: http://dx.doi.org/10.1175/MWR3466.1

Author Manuscript

This article is protected by copyright. All rights reserved.

Author Manuscript

Figure Captions

Figure 1: Ordinate axis gives the value of the models "zonal-wind/current-like" variables at each of the levels. Position on abscissa axis gives the intended horizontal location of the model variable while the number on the abscissa axis gives the horizontal index of the associated grid point. Red line gives an initial true state of the idealized coupled model. Black lines give individual ensemble members obtained by randomly sampling the climatology of the model. The yellow line gives the mean of this ensemble. Cyan crosses give the locations and values of error

This article is protected by copyright. All rights reserved.

prone observations of the true state. Observation locations randomly move for each data assimilation cycle.

Figure 2: Abscissa gives time in days. Ordinate gives the variance. Thick black line gives the temporal evolution of the horizontal average of the sample variance of a 16 member ensemble that was designed to indicate the predictability of the idealized coupled model. This ensemble was initialized by adding very small random perturbations to the true state at t=0 days. The thin line gives the evolution of the horizontal average of the mean square difference between the ensemble mean and the true state.

Figure 3: In a 2D model, the evolution of the target variable T_{33} over a single time step would be solely determined by the variables within some finite influence region surrounding it.

Figure 4: Thin black line gives the difference $\delta\mathbf{x}_{120}^{test}$ between a very slightly perturbed and an unperturbed non-linear trajectory after 5 days (120 hrs) of integration with a 6 hr time step. In the limit of a vanishingly small perturbation, the true TLM would perfectly predict this line. The red line is the prediction $\delta\mathbf{x}_{120}^{LETLM}$ of the black line given by the LETLM with just 28 members. Because the LETLM is so accurate, the black line is almost entirely obscured by the red line. The

Author Manuscript

This article is protected by copyright. All rights reserved.

thin blue line gives the very poor prediction obtained if the ETLM does not use any localization and only 28 ensemble members are used. The thick cyan line gives the very accurate prediction from an ETLM that uses an ensemble so large (480 members) that no localization is necessary.

Figure 5: Solid line gives the sensitivity of the 12 hr forecast of the 50^{th} variable in the oceanic boundary layer to changes in the initial condition. The vertical line in the 3^{rd} panel serves to mark the location of the forecast variable whose gradient is given by the solid line.

Figure 6: As in Figure 5, but for a 5 day forecast.

Figure 7: Convergence of mean square error (the ordinate axis) of the 4DVAR four-dimensional guess trajectory from 0 hr to 120 hrs in 6 hr intervals as a function of outer-loop iteration number (the abscissa axis) for LETLM enabled strong-constraint 4DVAR over 10 outer loops.

Figure 8: The green line is the posterior mode obtained from strong-constraint 4DVAR after 10 outer loops at the end of the 5 day data assimilation window. The red line is the true state but is obscured at locations where the posterior mode analysis is very accurate and lies on top of it. Cyan "+" signs give the values of the observations that were taken on day 5.

Figure 9: As in Figure 8, but for the middle of the data assimilation window. Note that the observations are at different sites to those depicted in Figure 8 because the observation locations shift randomly from one time step to the next.

Author Manuscript

This article is protected by copyright. All rights reserved.

Figure 10: As in Figure 8, but at 6 hr. Note that the observations are at different sites to those depicted in Figures 8 and 9 because the observation locations shift randomly from one time step to the next.

Figure 11: The left panels show the LETLM predicted error correlation function between a 5 day forecast error of variable 50 of the oceanic boundary layer (indicated by the vertical line) and the initial time errors of every single model variable. Specifically, it is a 4D correlation function of a 480 member ensemble forecast made by propagating the initial ensemble perturbations forward in time using the LETLM. The right panels show the 4D correlation function of a 480 member ensemble forecast made from the same initial conditions as that used to generate the left panels but for the right panels, the non-linear model was used to generate the ensemble forecast.

Figure 12: Initial time error correlation function of all initial variables with variable 10 of the atmospheric boundary layer.

Author Manuscript

This article is protected by copyright. All rights reserved.

Figures

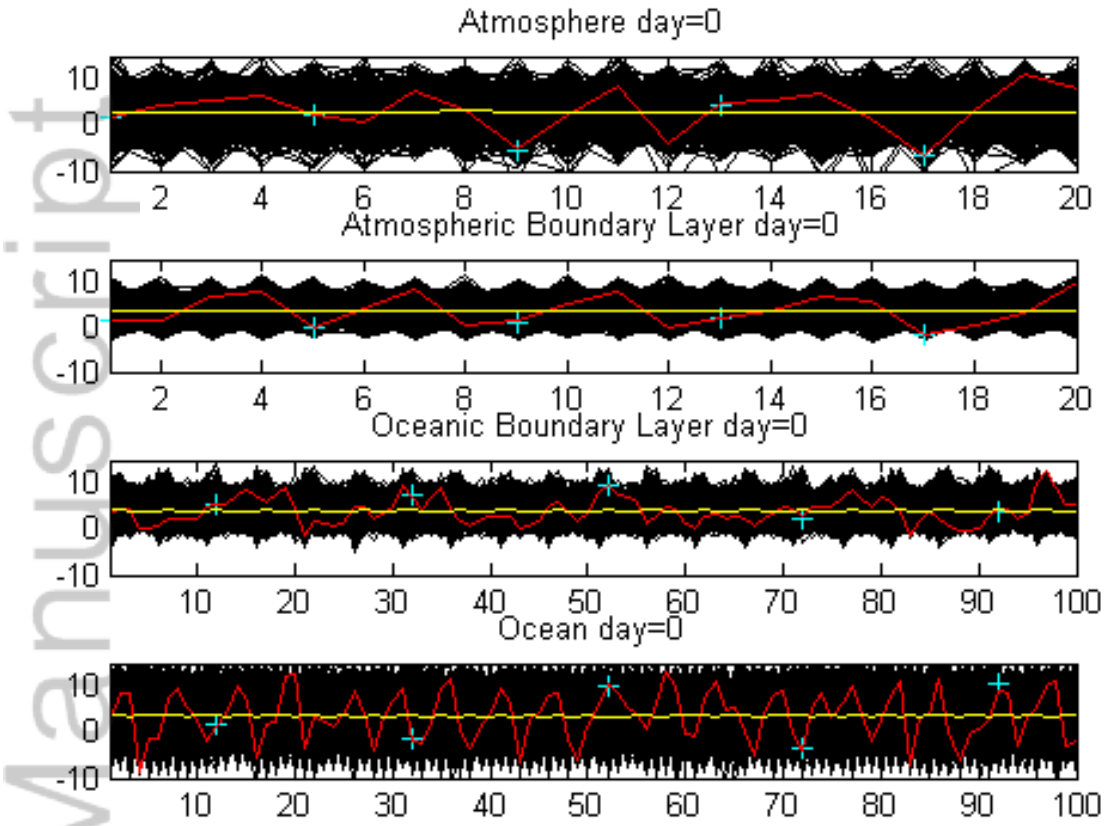

Figure 1: Ordinate axis gives the value of the models "zonal-wind/current-like" variables at each of the levels. Position on abscissa axis gives the intended horizontal location of the model variable while the number on the abscissa axis gives the horizontal index of the associated grid point. Red line gives an initial true state of the idealized coupled model. Black lines give individual ensemble members obtained by randomly sampling the climatology of the model. The yellow line gives the mean of this ensemble. Cyan crosses give the locations and values of error prone observations of the true state. Observation locations randomly move for each data assimilation cycle.

Author Manuscript

This article is protected by copyright. All rights reserved.

Author Manuscript

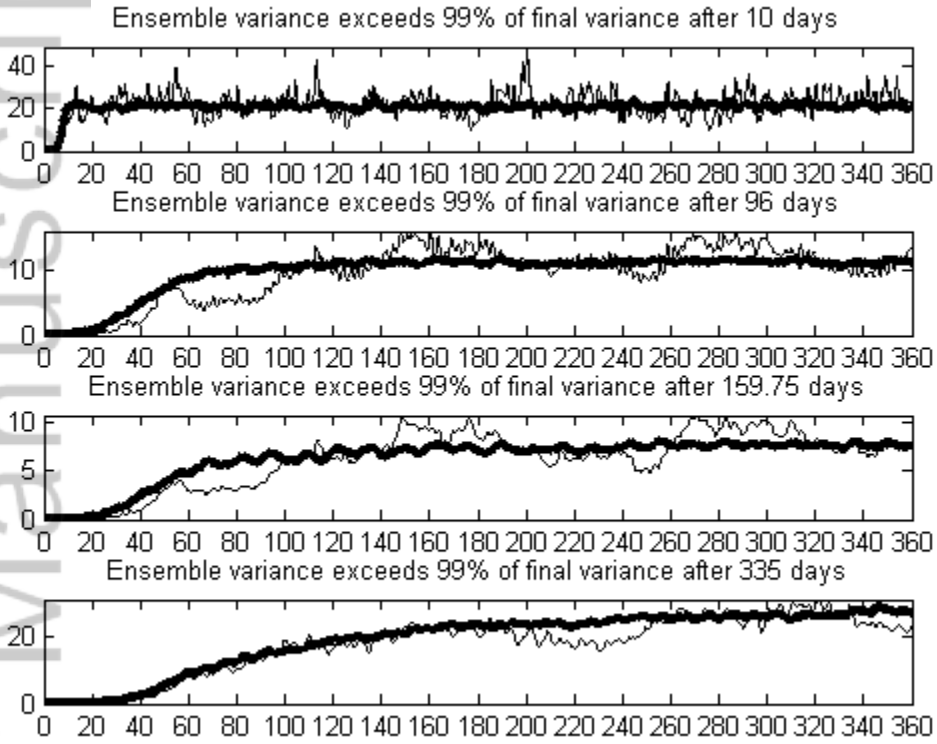

Figure 2: Abscissa gives time in days. Ordinate gives the variance. Thick black line gives the temporal evolution of the horizontal average of the sample variance of a 16 member ensemble that was designed to indicate the predictability of the idealized coupled model. This ensemble was initialized by adding very small random perturbations to the true state at t=0 days. The thin line gives the evolution of the horizontal average of the mean square difference between the ensemble mean and the true state.

This article is protected by copyright. All rights reserved.

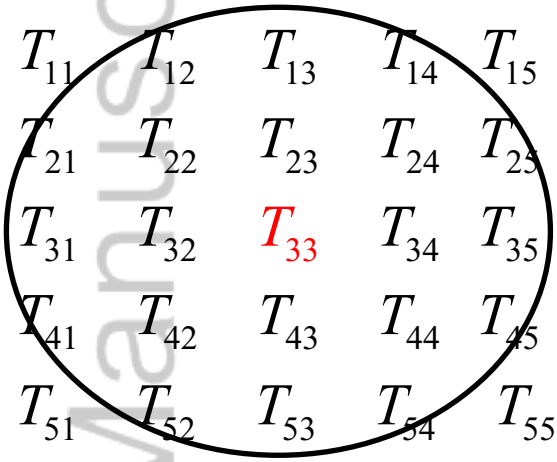

Figure 3: In a 2D model, the evolution of the target variable T_{33} over a single time step would be solely determined by the variables within some finite influence region surrounding it.

Author Manuscript

This article is protected by copyright. All rights reserved.

Author Manuscript

This article is protected by copyright. All rights reserved.

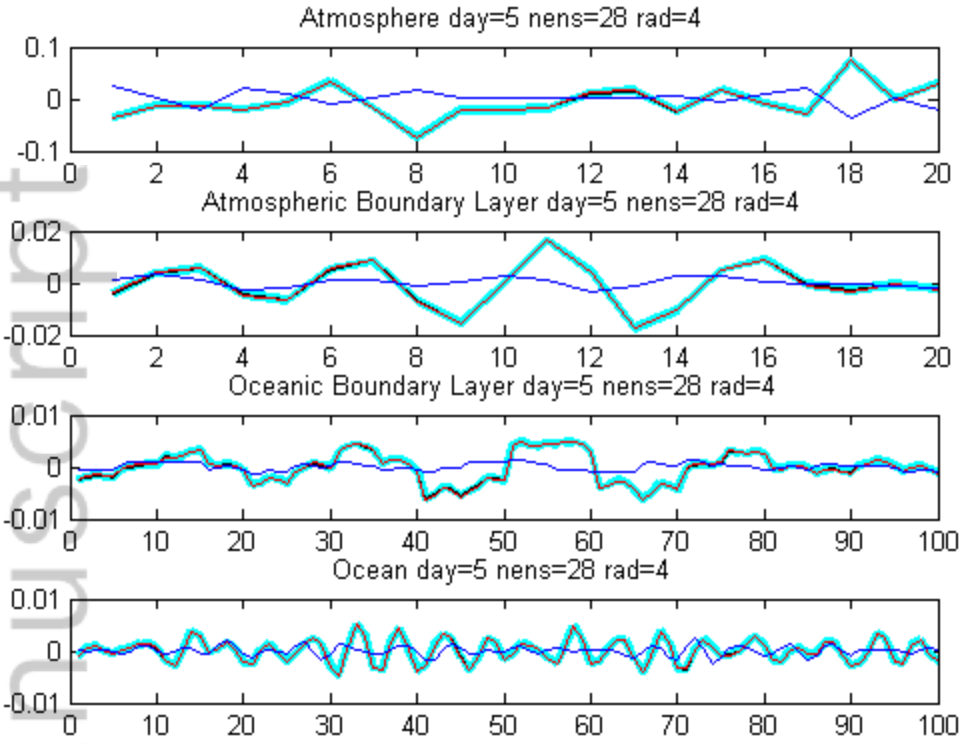

Figure 4: Thin black line gives the difference $\delta \mathbf{x}_{120}^{test}$ between a very slightly perturbed and an unperturbed non-linear trajectory after 5 days (120 hrs) of integration with a 6 hr time step. In the limit of a vanishingly small perturbation, the true TLM would perfectly predict this line. The red line is the prediction $\delta \mathbf{x}_{120}^{LETLM}$ of the black line given by the LETLM with just 28 members. Because the LETLM is so accurate, the black line is almost entirely obscured by the red line. The thin blue line gives the very poor prediction obtained if the ETLM does not use any localization and only 28 ensemble members are used. The thick cyan line gives the very accurate prediction from an ETLM that uses an ensemble so large (480 members) that no localization is necessary.

Author Manuscript

This article is protected by copyright. All rights reserved.

Author Manuscript

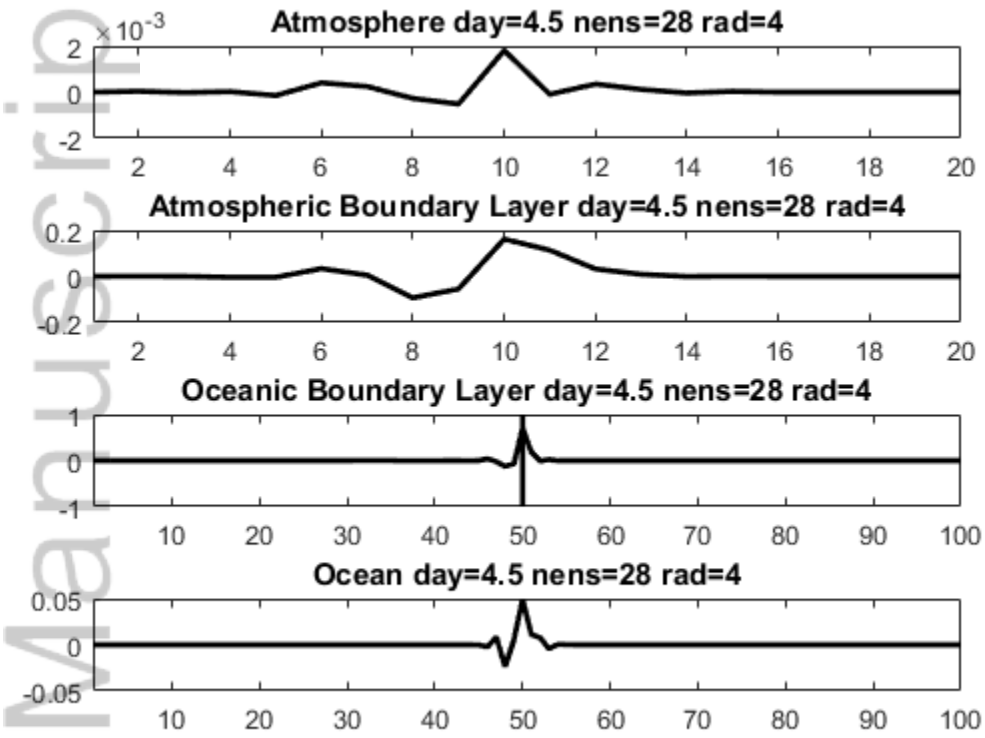

Figure 5: Solid line gives the sensitivity of the 12 hr forecast of the 50th variable in the oceanic boundary layer to changes in the initial condition. The vertical line in the 3rd panel serves to mark the location of the forecast variable whose gradient is given by the solid line.

This article is protected by copyright. All rights reserved.

Author Manuscript

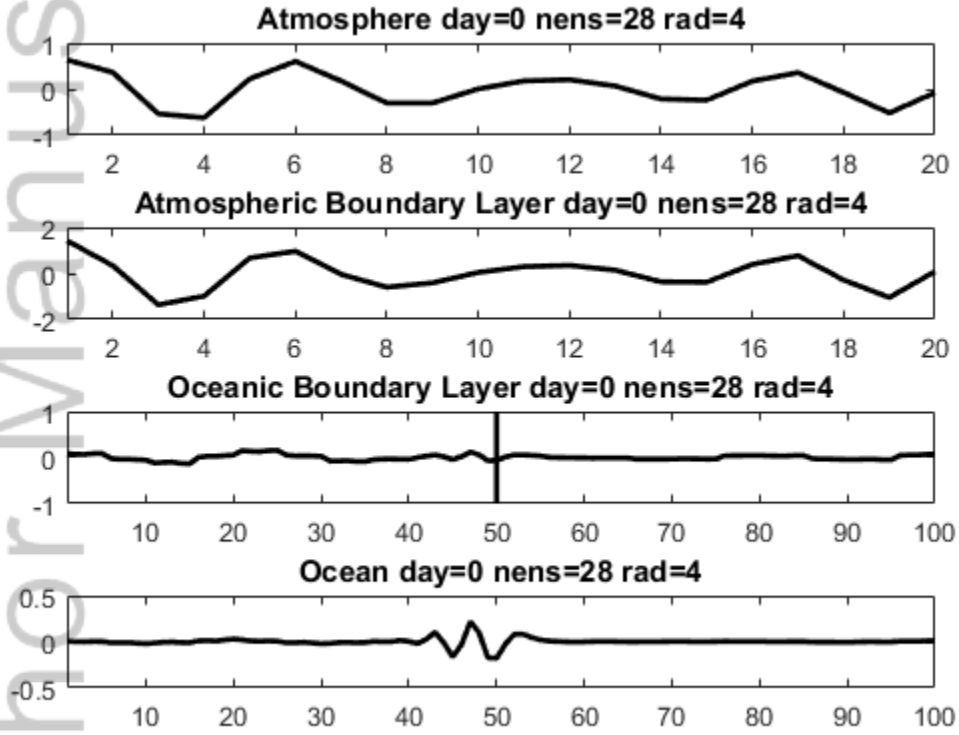

Figure 6: As in Figure 5, but for a 5 day forecast.

This article is protected by copyright. All rights reserved.

Author Manuscript

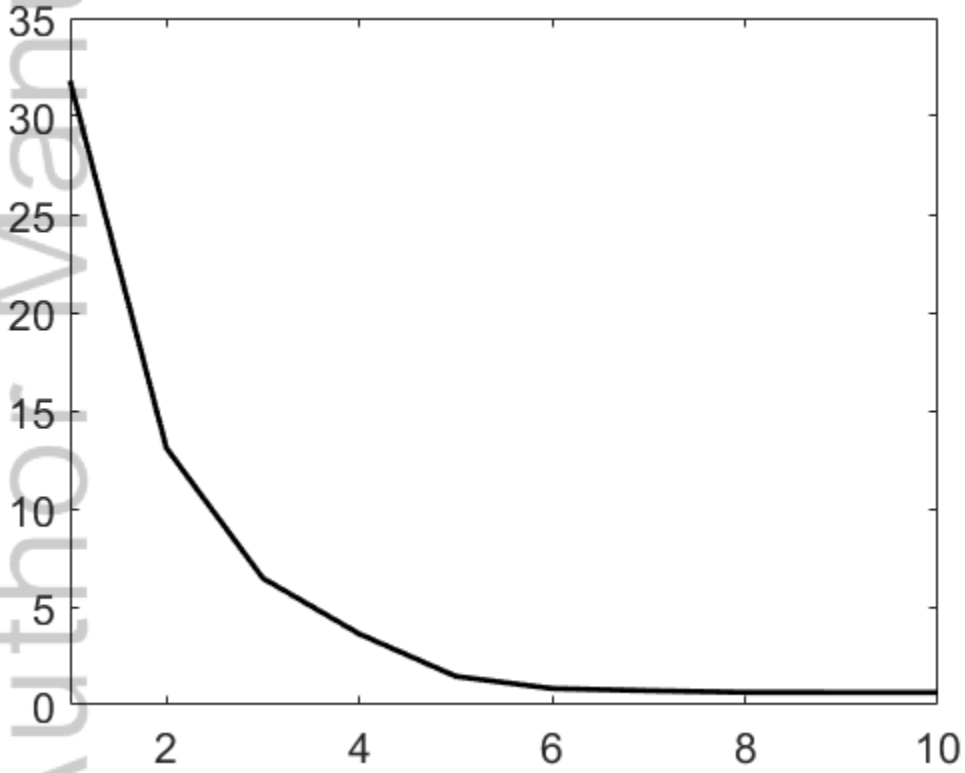

This article is protected by copyright. All rights reserved.

Figure 7: Convergence of mean square error (the ordinate axis) of the 4DVAR four-dimensional guess trajectory from 0 hr to 120 hrs in 6 hr intervals as a function of outer-loop iteration number (the abscissa axis) for LETLM enabled strong-constraint 4DVAR over 10 outer loops.

Author Manuscript

This article is protected by copyright. All rights reserved.

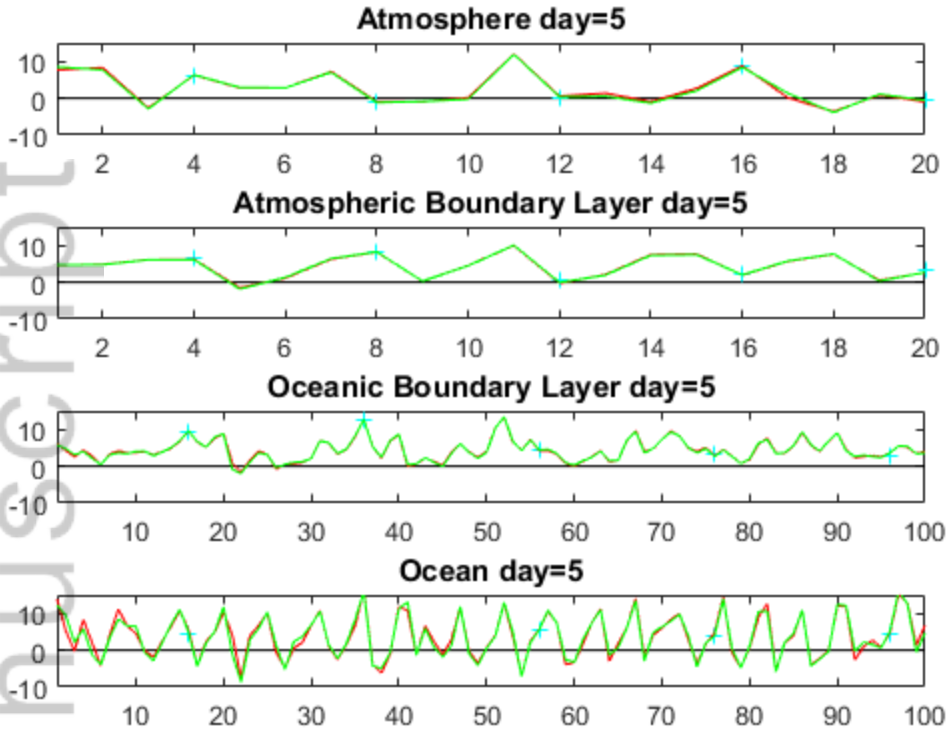

Figure 8: The green line is the posterior mode obtained from strong-constraint 4DVAR after 10 outer loops at the end of the 5 day data assimilation window. The red line is the true state but is obscured at locations where the posterior mode analysis is very accurate and lies on top of it. Cyan "+" signs give the values of the observations that were taken on day 5.

Author Manuscript

This article is protected by copyright. All rights reserved.

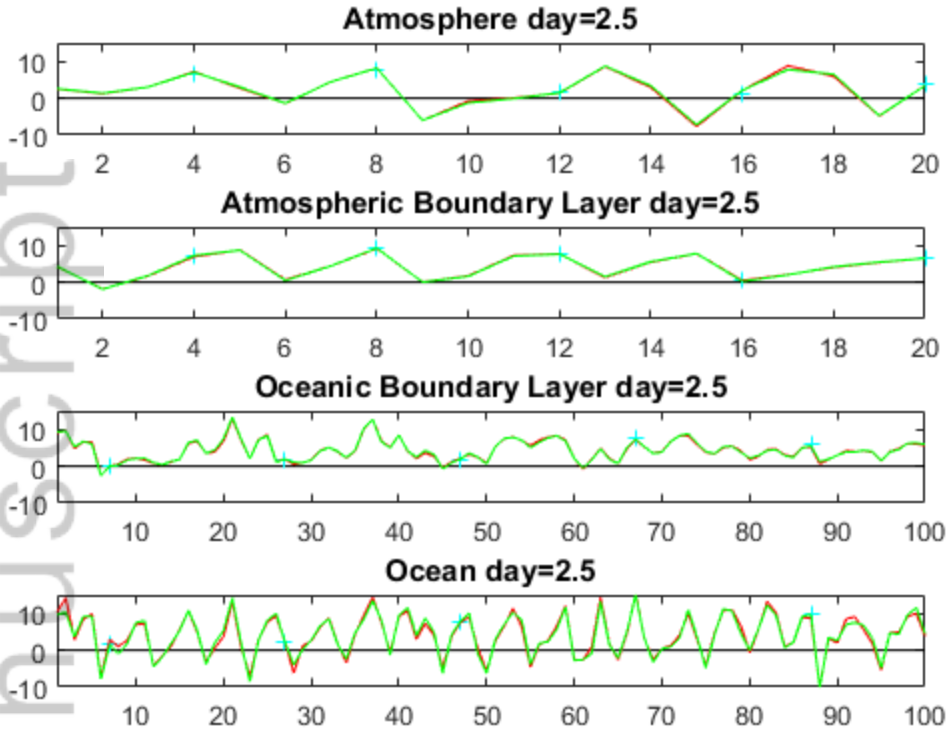

Figure 9: As in Figure 8, but for the middle of the data assimilation window. Note that the observations are at different sites to those depicted in Figure 8 because the observation locations shift randomly from one time step to the next.

Author Manuscript

This article is protected by copyright. All rights reserved.

Author Manuscript

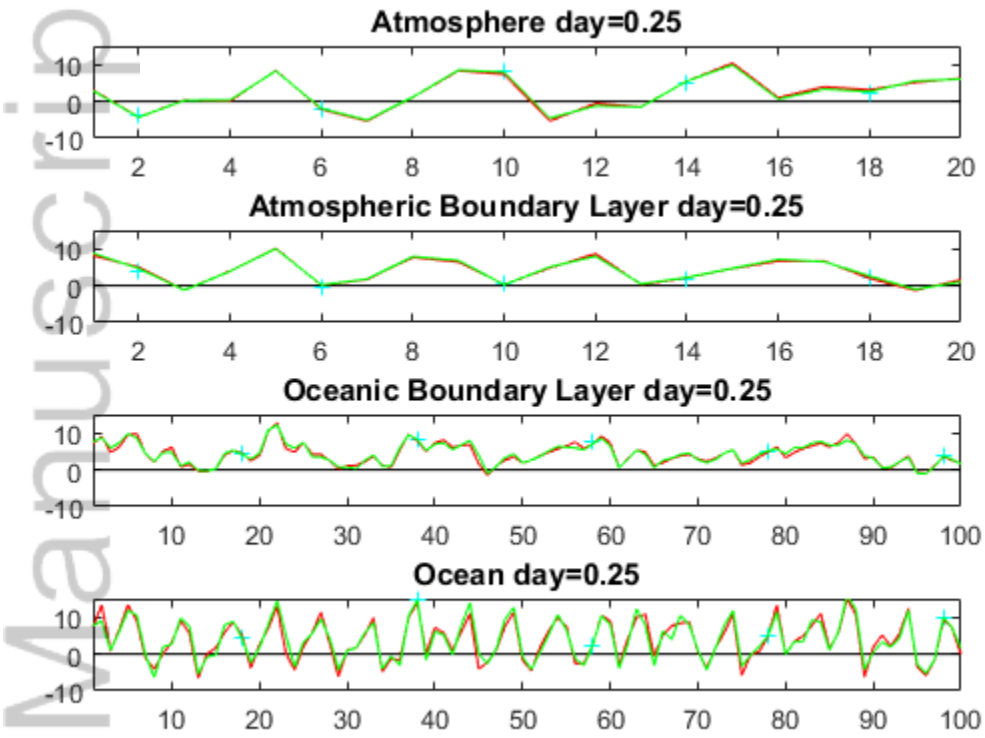

Figure 10: As in Figure 8, but at 6 hr. Note that the observations are at different sites to those depicted in Figures 8 and 9 because the observation locations shift randomly from one time step to the next.

This article is protected by copyright. All rights reserved.

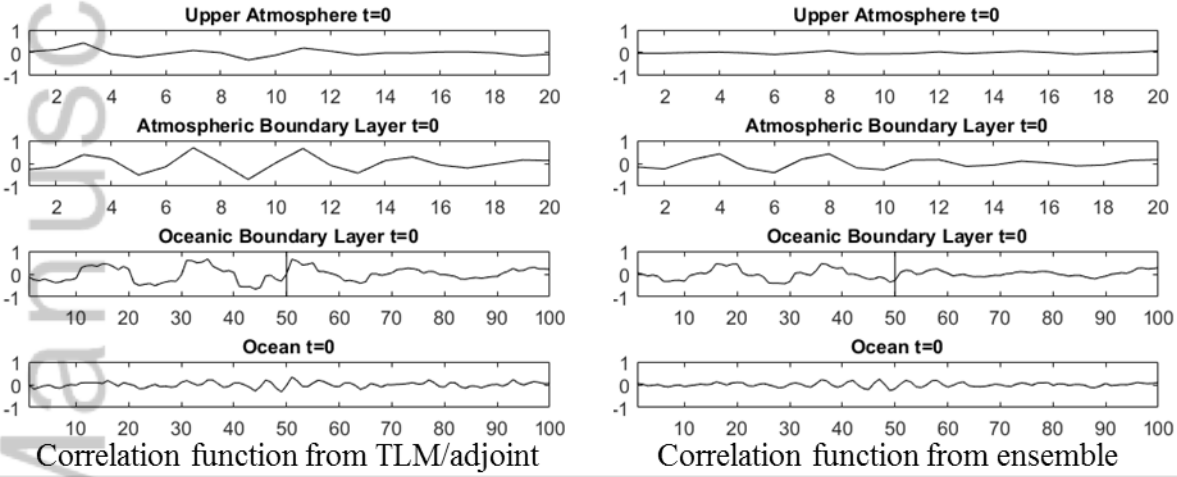

Figure 11: The left panels show the LETLM predicted error correlation function between a 5 day forecast error of variable 50 of the oceanic boundary layer (indicated by the vertical line) and the initial time errors of every single model variable. Specifically, it is a 4D correlation function of a 480 member ensemble forecast made by propagating the initial ensemble perturbations forward in time using the LETLM. The right panels show the 4D correlation function of a 480 member ensemble forecast made from the same initial conditions as that used to generate the left panels but for the right panels, the non-linear model was used to generate the ensemble forecast.

Author Manuscript

This article is protected by copyright. All rights reserved.

Author Manuscript

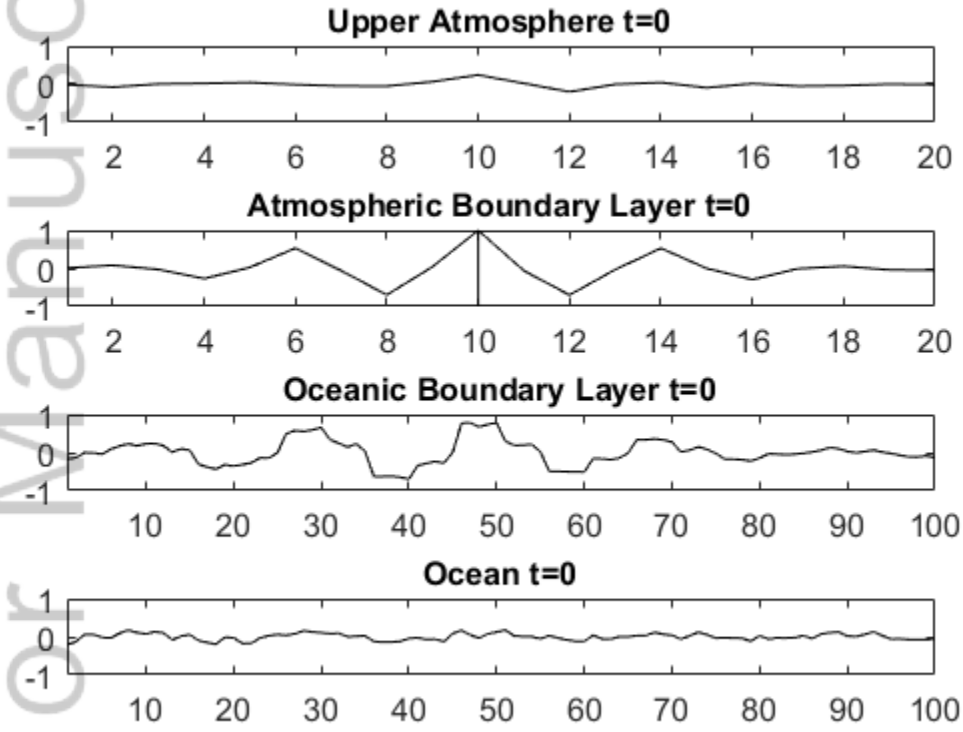

Figure 12: Initial time error correlation function of all initial variables with variable 10 of the atmospheric boundary layer.

This article is protected by copyright. All rights reserved.

Author Manuscript

This article is protected by copyright. All rights reserved.